(A proposal to Jefferson Lab PAC33)

Polarization transfer in Wide Angle Compton Scattering

A. Camsonne, J. P. Chen, E. Chudakov, C. DeJager, J. Gomez,
O. Hansen, D. W. Higinbotham, M. Jones, J. LeRose, R. Michaels, S. Nanda,
A. Saha, V. Sulkosky, S. A. Wood, B. Wojtsekhowski (spokesperson and contact person)
Thomas Jefferson National Accelerator Facility, Newport News, VA 23606

A. M. Nathan (spokesperson), M. Roedelbronn
University of Illinois, Champaign-Urbana, IL 61801

R. Gilman (spokesperson), G. Kumbartzki, R. Ransome, E. Schulte, J. Yuan
Rutgers, The State University of New Jersey, Piscataway, NJ 08854

D. J. Hamilton (spokesperson), J. R. M Annand, G. Rosner
University of Glasgow, Glasgow, Scotland

S. Abrahamyan, A. Ketikyan, A. Shahinyan, H. Voskanyan
Yerevan Physics Institute, Yerevan, Armenia

E. Cisbani, F. Cusanno, F. Garibaldi, S. Frullani, G. M. Urciuoli, M. Iodice
INFN, Rome, Italy

R. De Leo, L. La Gamba
INFN, Bari, Italy

D. Nikolenko, I. Rachek, Yu. Shestakov
Budker Institute, Novosibirsk, Russia

W. Boeglin, P. Markowitz
Florida International University, Miami, FL 33199

J. Calarco, W. Hersman
University of New Hampshire, Durham, NH 03824

M. Khandaker, V. Punjabi
Norfolk State University, Norfolk, VA 23504

B. Crowe, B. Vlahovic
North Carolina Central University, Durham, NC 03824

J. M. Laget, F. Sabatie
CEA Saclay, Gif-sur-Yvette, France

E. Piasetzky, G. Ron
Tel Aviv University, Israel

C. Perdrisat, L. Pentchev
College of William and Mary, Williamsburg, VA 23185

C. Hyde, A. Radyushkin
Old Dominion University

P. Kroll
Fachbereich Physik, Universitat Wuppertal, Germany

A. Vasiliev
IHEP, Protvino, Russia

D. Day, R. Lindgren, N. Liyanage, V. Mamyan, B. E. Norum
University of Virginia, Charlottesville, VA 22901

Z.-E. Meziani, B Sawatzky
Temple University, Philadelphia, PA 19122

and

The Hall A Collaboration

December 10, 2007

Contents

Abstract

An experiment is proposed to measure the components of the recoil proton polarization in Real Compton Scattering (RCS) with longitudinally polarized incident photons. Measurements are proposed at s= 9 (GeV/c)^2 for two values of the $\theta_p^{cm} = 90°$ and $110°$.

The recent JLab RCS experiment, E99-114, demonstrated the feasibility of the experimental technique and produced a remarkable result. Namely, at s= 7 (GeV/c)^2 and $\theta_p^{cm} = 120°$, the longitudinal polarization is in agreement with the handbag description of the process in which the photons interact with a single quark, but is completely inconsistent with a pQCD mechanism which involves three active quarks mediated by two hard gluon exchanges. It is essential to have additional **measurements at higher photon energy over a broader kinematic range** in order to identify the factorization regime and the reaction mechanism.

The experiment utilizes an untagged bremsstrahlung photon beam and the standard cryogenic target. The scattered photon is detected in the BigCal photon spectrometer, recently constructed and used by the GEP-III collaboration. The coincident recoil proton is detected in the Hall A magnetic spectrometer HRS-L or Hall C magnetic spectrometer HMS, and its polarization components are measured in the existing Focal Plane Polarimeters. With 508 hours of beam time in Hall A and 70 hours of beam time in Hall C, each of the three polarization observables, K_{LL}, K_{LT}, and P_N, will be measured to a statistical accuracy of ± 0.1 at each kinematic point.

Such a measurement would be of crucial importance for understanding of the reaction mechanism for this simplest process involving real photon and it is essential base for understanding of other photo-induced exclusive reactions in the JLab energy range.

1 Introduction

Compton scattering in the hard scattering limit is a powerful probe of the structure of the nucleon. Compton scattering in WACS regime provides access to the high t transverse structure of the hadron while in DVCS regime it provides access to the high Q^2 low t structure. It is a natural complement to other exclusive reactions, such as high Q^2 elastic electron scattering and high energy meson photo-production. Two photon couplings to the hadron allows to access the structure information which is not available from DIS and elastic electron scattering, at the same time data on RCS process likely more suitable for theoreticaly analysis then other photo reactions.

For Real Compton Scattering (RCS), the hard scale is achieved when s, $-t$, and $-u$ are all large compared to the proton mass, or equivalently, when the transverse momentum transfer $p_\perp$ is large. Under such conditions one expects the transition amplitude to factorize into the convolution of a perturbative hard scattering amplitude, which involves the coupling of the external photons to the active quarks, with an overlap of initial and final soft (nonperturbative) wave functions, which describes the coupling of the active quarks to the proton. Schematically this can be written

$$T_{if}(s,t) \;\; = \;\; \Psi_f \, \otimes \, K(s,t) \, \otimes \, \Psi_i \, , \tag{1}$$

where $K(s,t)$ is the perturbative hard scattering amplitude, and the Ψ's are the soft wave functions. Different factorization schemes have been applied to RCS in recent years and these can be distinguished by the number of active constituents participating in the hard scattering subprocess. The handbag mechanism [1, 2, 3] involves only one active constituent, while the perturbative QCD (pQCD) mechanism [4, 5, 6, 7, 8] involves three. In any given kinematic regime, both mechanisms will contribute, in principle, to the scattering amplitude. At "sufficiently high" energy, the pQCD mechanism is expected to dominate, but it is not known how high is sufficiently high or the manner in which the transition to the purely pQCD mechanism emerges. Duality considerations were applied to RCS process [9]. Diquark approach was also successful in description of the WACS cross section [10].

At relatively low energy (e.g., in the resonance region), RCS and other exclusive reactions are dominated by purely soft physics, and the amplitude does not factorize into hard and soft processes. At high energy but small $-t$ or $-u$, soft physics also dominates through Regge exchanges [11]. The nature of the transition from purely soft to the factorization regime is also not well known. Quite aside from the reaction mechanism, it is of interest to ask what RCS can teach us about the nonperturbative structure of the proton and to relate it to that revealed in other reactions.

With this backdrop, experiment E99-114 [12] was undertaken to study the RCS reaction. The primary focus was the measurement of precise spin-averaged cross sections over the kinematic regime of $5 \le s \le 11$ (GeV/c)^2 and $1.5 \le -t \le 6.5$ (GeV/c)^2. In addition, a measurement was made at a single kinematic point of the polarization transfer to the recoil proton using longitudinally polarized incident photons. The latter measurement has produced a remarkable result [13], which is shown in Fig. 1 and which will be discussed in more detail in the next section of this proposal. Namely, the longitudinal polarization transfer is consistent with the handbag and Regge exchange predictions and completely inconsistent with predictions based on pQCD. This gives very strong credence to the notion that the photons interact with a single quark. Indeed, the longitudinal polarization is nearly as large as that expected for scattering from a free quark. However, we strongly emphasize that this is a measurement at a *single kinematic point*, and that the factorization regime might not have been reached in this case since the corresponding value of u was only -1.1 (GeV/c)^2. It is essential to verify and improve upon this result with measurements over a broader kinematic range. It is also very important to perform measurements at higher photon energy, so that the factorization condition that all kinematic Al variables are much larger than the proton mass is unequivocally met.

It should be noted that the proposed measurement is part of a broader experimental program involving RCS at JLab. Two further experiments have been approved for beam time in Hall C, one of which is a complementary measurement of recoil polarization observables at $s = 9$ (GeV/c)^2 and θ_p^{cm}= 70° using BigCal and the HMS [14], while the other involves utilization of a polarized target in order to extract the beam-target double polarization observables A_{LL} and A_{LT} [15] at a photon energy of $E_\gamma = 4.3$ GeV. Moreover, the 12 GeV upgrade will open up an entirely new kinematic regime for RCS cross section measurements, a regime in which the contribution from factorization along pQCD lines should be much more pronounced.

We propose new measurements of polarization observables in Compton scattering at an incident energy of 4.3 GeV, or s=9 (GeV/c)^2, at scattering angles of θ_p^{cm}= 90 and 110°. The proposal is organized as follows. In Section 2 we present our physics motivation and summarize the physics goals of the proposed experiment. In Section 3 we describe the experimental approach and both the standard and the specialized equipment. In subsequent sections, we present our proposed measurements (Sec. 4), our expected results and beam time request (Sec. 5), and the technical considerations related to the equipment and the experiment schedule (Sec. 7). The proposal is summarized in Section 8.

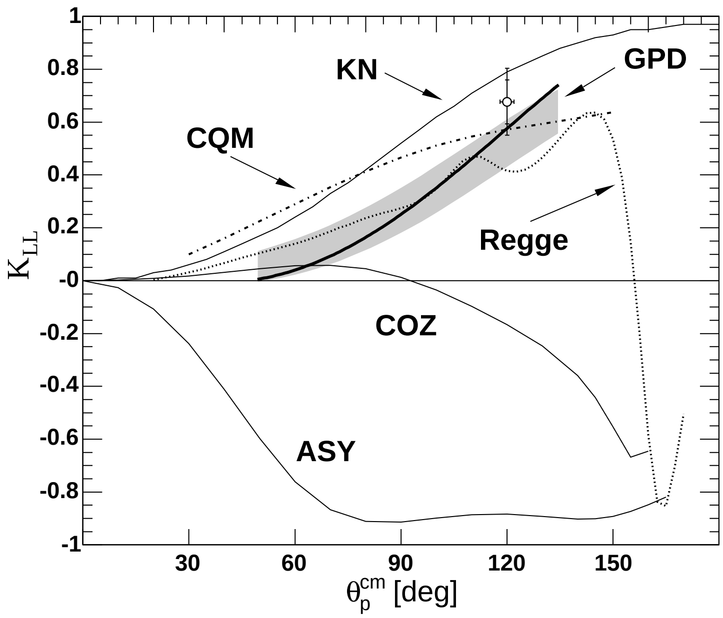

Figure 1: Longitudinal polarization transfer in the RCS process at an incident energy of 3.23 GeV [13]. The labels on the curves are KN for the asymmetry in the hard subprocess; GPD, shown as a gray band, for the handbag approach using GPD's [16]; CQM for the handbag approach using constituent quarks [17]; Regge for a Regge exchange mechanism [18]; and COZ and ASY for pQCD calculations [7] using the asymptotic (ASY) or Chernyak-Ogloblin-Zhitnitsky (COZ) distribution amplitudes.

2 Physics Motivation

2.1 Overview

In view of the remarks in the Introduction, we consider several interesting questions that motivate us to explore further the measurement of polarization observables in RCS at JLab:

1. Is it indeed true that the RCS reaction proceeds through the interaction of the photons with a single quark?
2. What information can be learnt about the structure of the proton from new measurements of the polarization observables and how is this structure related to that measured in other exclusive reaction?
3. At what kinematic scale is factorization into hard and soft process valid?

In order to present a framework for addressing these issues, we next present discussions of three reaction mechanisms: the handbag, pQCD, and Regge exchange mechanisms.

2.2 Handbag Mechanism in GPD-based Models

The handbag mechanism offers new possibilities for the interpretation of hard exclusive reactions. For example, it provides the framework for the interpretation of so-called deep exclusive reactions, which are reactions initiated by a high-Q^2 virtual photon. The application of the formalism to RCS (see Fig. 2) was initially worked out to leading order (LO) by Radyushkin [1] and subsequently by Diehl [2]. More recently next-to-leading-order (NLO) contributions have been worked out by Huang and Kroll [3]. The corresponding diagram for elastic electron scattering is similar to Fig. 2, except that there is only one external virtual photon rather than two real photons. In the handbag approach, the hard physics is contained in the scattering from a single active quark and is calculable using pQCD and QED: it is just Compton scattering from a structureless spin-1/2 particle. The soft physics is contained in the wave function describing how the active quark couples to the proton. This coupling is described in terms of GPD's. The GPD's have been the subject of intense experimental and theoretical activity in recent years [19, 20]. They represent "superstructures" of the proton, from which are derived other measurable structure functions, such as parton distribution functions (PDF) and form factors. To NLO, only three of the four GPD's contribute to the RCS process: $H(x, \xi = 0, t)$, $\hat{H}(x, \xi = 0, t)$, and $E(x, \xi = 0, t)$. Since the photons are both real, the so-called skewness parameter ξ=0, reflecting the fact that the momentum absorbed by the struck quark is purely transverse. In the handbag formalism, the RCS observables are new form factors of the proton that are x^{-1}-moments of the GPD's:

$$
\begin{aligned}
R_V(t) &= \sum_a e_a^2 \int_{-1}^{1} \frac{dx}{x} H^a(x, 0, t), \\
R_A(t) &= \sum_a e_a^2 \int_{-1}^{1} \frac{dx}{x}\, sign(x)\, \hat{H}^a(x, 0, t),
\end{aligned}
$$

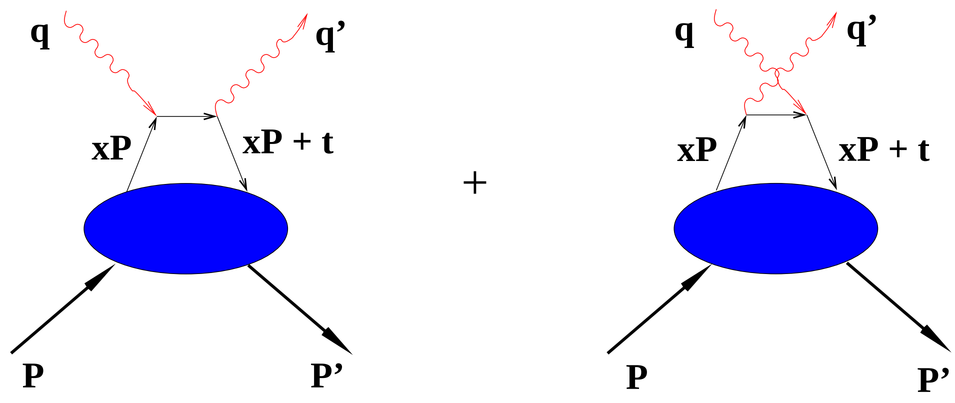

Figure 2: The handbag diagram for RCS.

$$R_T(t) \;=\; \sum_a e_a^2 \int_{-1}^{1} \frac{dx}{x} E^a(x,0,t),$$

where e_a is the charge of the active quark and the three form factors are, respectively, the vector, axial vector, and tensor form factors. The corresponding form factors for elastic electron or neutrino scattering are given by the x^0-moments of the same GPD's:

$$\begin{aligned} F_1(t) &= \sum_a e_a \int_{-1}^{1} dx\, H^a(x,0,t), \\ G_A(t) &= \sum_a \int_{-1}^{1} dx\, sign(x)\, \hat{H}^a(x,0,t), \\ F_2(t) &= \sum_a e_a \int_{-1}^{1} dx\, E^a(x,0,t), \end{aligned}$$

where the three quantities are, respectively, the Dirac, axial, and Pauli form factors. On the other hand, the $t = 0$ limit of the GPD's produce the PDF's:

$$\begin{aligned} H^a(x,0,0) &= q^a(x), \\ \hat{H}^a(x,0,0) &= \Delta q^a(x) \\ E^a(x,0,0) &= 2\frac{J^a(x)}{x} - q^a(x), \end{aligned} \tag{2}$$

where J^a is the total angular momentum of quark flavor a and is not directly measurable in DIS.

In the handbag factorization scheme, the RCS helicity amplitudes are related to the form factors by

$$
\begin{aligned}
M_{\mu'+,\mu+}(s,t) &= 2\pi\alpha_{em}\left[T_{\mu'+,\mu+}(s,t)(R_V(t)+R_A(t))+T_{\mu'-,\mu-}(s,t)(R_V(t)-R_A(t))\right], \\
M_{\mu'-,\mu+}(s,t) &= 2\pi\alpha_{em}\frac{\sqrt{-t}}{m}\left[T_{\mu'+,\mu+}(s,t)+T_{\mu'-,\mu-}(s,t)\right]R_T(t),
\end{aligned}
$$

where μ, μ' denote the helicity of the incoming and outgoing photons, respectively. The signs on M and T refer to the helicities of the proton and active quark, respectively. This structure of the helicity amplitudes leads to a simple interpretation of the RCS form factors: $R_V \pm R_A$ is the response of the proton to the emission and re-absorption of quarks with helicity in the same/opposite direction of the proton helicity, and R_T is directly related to the proton helicity-flip amplitude [3].

These equations leads to expressions relating RCS observables to the form factors. The most important of these experimentally are the spin-averaged cross section and the recoil polarization observables. The spin-averaged cross section factorizes into a simple product of the Klein-Nishina (KN) cross section describing the hard scattering from a single quark and a sum of form factors depending only on t [1, 2]:

$$
\frac{d\sigma/dt}{d\sigma_{\rm KN}/dt} = f_V\left[R_V^2(t) + \frac{-t}{4m^2}R_T^2(t)\right] + (1-f_V)R_A^2(t)\,, \tag{3}
$$

For the the interesting region of large $p_\perp$, the kinematic factor f_V is always close to 1. Consequently the unpolarized cross sections are largely insensitive to R_A, and the left-hand-side of Eq. 3 is nearly s-independent at fixed t. The recent calculations to NLO, which take into account both photon and proton helicity-flip amplitudes, do not change this prediction in any appreciable way [3]. The polarization transfer observables, K_{LL} and K_{LT}, respectively, are defined by

$$
K_{LL}\frac{d\sigma}{dt} \equiv \frac{1}{2}\left[\frac{d\sigma(\uparrow\downarrow)}{dt} - \frac{d\sigma(\uparrow\downarrow)}{dt}\right] \qquad K_{LT}\frac{d\sigma}{dt} \equiv \frac{1}{2}\left[\frac{d\sigma(\uparrow\rightarrow)}{dt} - \frac{d\sigma(\downarrow\rightarrow)}{dt}\right] \tag{4}
$$

where the first arrow refers to the incident photon helicity and the second to the recoil proton helicity ($\uparrow$) or transverse polarization ($\rightarrow$). The induced polarization of the recoil proton normal to the scattering plane, P_N, is defined by

$$
P_N\frac{d\sigma}{dt} \equiv \frac{1}{2}\left[\frac{d\sigma(\uparrow)}{dt} - \frac{d\sigma(\downarrow)}{dt}\right] \tag{5}
$$

and is independent of the incident photon polarization. Here $\uparrow$ and $\downarrow$ denote the component of polarization up and down, respectively, with respect to the scattering plane. With definitions of two additional parameters

$$
\beta = \frac{2m}{\sqrt{s}}\frac{\sqrt{-t}}{\sqrt{s}+\sqrt{-u}} \qquad \kappa(t) = \frac{\sqrt{-t}}{2m}\frac{R_T(t)}{R_V(t)}\,, \tag{6}
$$

the three polarization observables are approximately related to the form factors by the expressions [2, 3]

$$K_{LL} \approx K_{LL}^{\rm KN} \frac{R_A(t)}{R_V(t)} \frac{1-\beta\kappa(t)}{1+\kappa^2(t)} \qquad \frac{K_{LT}}{K_{LL}} \approx \kappa(t) \frac{1+\beta\kappa^{-1}(t)}{1-\beta\kappa(t)} \qquad P_N \approx 0\,, \tag{7}$$

where $K_{LL}^{\rm KN}$ is the longitudinal asymmetry for a structureless Dirac particle. These formulae do not include small gluonic corrections, which are discussed in Ref. [3].

From the relationships connecting RCS form factors to PDF's, Eq. 2, the ratio R_A/R_V is related to $\Delta q^a(x)/q^s(x)$. For RCS, the e_a^2-weighting of the quark flavors means that u quarks will dominate the reaction. Moreover, at moderate-to-high $-t$, the contributions to the form-factor integral are concentrated at moderate-to-high x, where the valence quarks dominate. Therefore, the K_{LL} asymmetry has direct information on $\Delta u(x)/u(x)$ in the valence region. Obtaining this kind of information is one of the key justifying physics goals for a possible 12 GeV upgrade of JLab.

From the correspondence between RCS and electron scattering form factors, there is expected to be a close relationship between R_T/R_V and F_2/F_1 [3]. The JLab G_E^p experiments [21, 22] have shown that F_2/F_1 falls as $1/\sqrt{-t}$ rather than as $1/t$, the latter being predicted by pQCD. It will be an important check on the theoretical interpretation of F_2/F_1 to see if R_T/R_V behaves in a similar way. In the current context, this means that the parameter $\kappa(t)$, and therefore K_{LT}/K_{LL}, would be nearly independent of t. We will investigate this in the proposed experiment, up to $-t = 5$ /(GeV/c)^2. The results from E99-114 at $-t = 4$ are consistent with $R_T/R_V \approx (0.6\pm\ 0.3)F_2/F_1$. Although the uncertainties are large, this result suggests that R_T/R_V may fall more rapidly with $-t$ than F_2/F_1. One of the goals of the proposed experiment is to obtain better precision on K_{LT}.

Finally, we note that the quantity P_N is predicted to vanish to NLO, except for possible gluonic contributions, which involve additional (unknown) soft form factors [3]. These contributions have been estimated to contribute no more than about 0.03 to P_N. An accurate experimental determination of P_N will be helpful in obtaining better estimates of the gluonic contributions to both K_{LL} and K_{LT}.

2.3 Handbag Mechanism in a Relativistic Constituent Quark Model

A different formulation for RCS in the handbag approach that varies significantly from the GPD formalism described above is that of Miller [17]. In his approach the handbag diagram involves γq scattering, as before, and proton wave functions obtained from relativistic Constituent Quark Models (CQM). What distinguishes this approach from the both the Leading Order GPD and pQCD models is the fact that these proton wave functions explicitly include the influence of quark transverse momenta and configurations involving non-zero quark orbital angular momentum. This naturally corresponds to violation of proton helicity conservation. Indeed, non-conservation of proton helicity in this model has proved to be one of the key factors in its successful account of electromagnetic form factor data for the proton [23, 24].

The calculations for RCS involve evaluating the handbag diagrams of Fig. 2 in an impulse approximation. The resultant reaction amplitude depends on proton wave functions obtained from Poincaré invariant calculations involving constituent quark models in light-front dynamics. These wave functions have previously been constrained by proton electromagnetic form factor data in the same kinematic regime [24]. Significant contributions to the wave functions from quark transverse momenta and orbital angular momentum are direct artifacts of the relativistic nature of the calculations.

Reasonable agreement with RCS cross section data has been obtained with a slight modification of the constituent quark masses [17]. In the case of the RCS spin observables, a similar large value of K_{LL} as for the GPD approach (see Fig.1), and a value for the transverse polarization transfer of $K_{LT}= 0$ have been predicted. Unlike in the GPD case given above, where P_N is predicted to be close to zero, the induced proton polarization in the CQM approach varies from a large positive value at forward scattering angles to a large negative value at backward angles. This is a direct consequence of proton helicity flip, and therefore of significant contributions from states with non-zero quark orbital angular momentum, and is justification for further measurements of P_N in this kinematic regime.

2.4 pQCD Mechanism

The traditional framework for the interpretation of hard exclusive reactions has been perturbative QCD (pQCD) [25]. This is based in part on the observation that the onset of scaling in Deep Inelastic Scattering (DIS) occurs at the relatively low scale of $Q^2 \sim 1$–2 (GeV/c)^2, thereby giving rise to expectations that pQCD might also be applicable to the exclusive processes in the range of a few $(\mathrm{GeV}/c)^2$. The pQCD approach to RCS [4, 5, 6, 7, 8] is shown in Fig. 3, where it is seen that the three valence quarks are active participants in the hard subprocess, which is mediated by the exchange of two hard gluons. The soft physics is contained in the so-called valence quark distribution amplitudes. The pQCD mechanism leads naturally to the so-called constituent counting rules for exclusive processes:

$$\frac{d\sigma}{dt} = \frac{f(\theta_{cm})}{s^n}, \tag{8}$$

where n is related to the number of active constituents in the reaction [26, 27]. Indeed, the observation that many exclusive reactions, such as elastic electron scattering, pion photoproduction, and RCS, approximately obey Eq.8 has led to the belief that the pQCD mechanism dominates at experimentally accessible energies. There seems to be little theoretical disagreement that the pQCD mechanism dominates at sufficiently high energies [28]; however, there is no consensus on how high is "sufficiently high." Indeed, despite the observed scaling, absolute cross sections calculated using the pQCD framework are very often low compared to existing experimental data, sometimes by more than an order of magnitude. Moreover, several recent JLab experiments that measure polarization observables also disagree with the predictions of pQCD. In the G_E^p experiment [21, 22] the slow falloff of the Pauli form factor $F_2(Q^2)$ up to Q^2 of 5.5 $(\mathrm{GeV}/c)^2$ provides direct evidence that hadron helicity is not conserved, contrary to predictions of pQCD. Similar findings were made in the π^0 photo-production experiment [29], where both the non-zero transverse and normal components of polarization of the recoil proton are indicative of hadron helicity-flip, which is again contrary to the predictions of pQCD. Finally, in the recently completed RCS experiment, E99-114, the preliminary analysis of the longitudinal polarization transfer K_{LL} (which will be defined precisely below) shows a value which is large and positive, contrary to the pQCD prediction which is negative. Moreover, the E99-114 data are consistent with a scaling factor $n \approx 8$ rather than the value $n = 6$, which is expected from pQCD and was consistent with earlier, less precise data [30] (see Fig. 4).

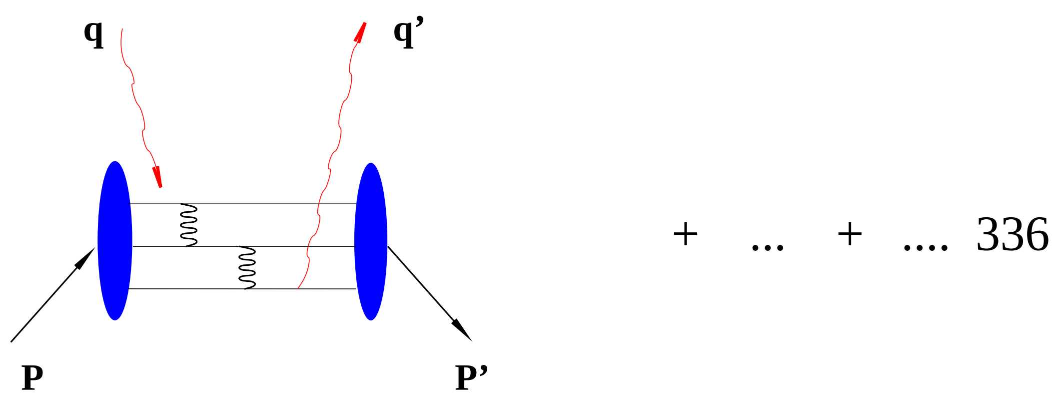

Figure 3: Two gluon exchange pQCD diagram (plus 336 similar configurations) for RCS.

A recalculation of the pQCD mechanism and reassessment in light of the E99-114 data has recently been completed by Thompson et al. [8]. It is argued in this work that K_{LL} should be measured in a regime where the kinematical variables are all significantly larger than the proton mass scale, which was not the case in E99-114. They further argue that the observed decrease in the scaled cross section as s increases is consistent with a view that the onset of an asymptotic regime will soon be accessible. Moreover, some commonality between the pQCD and handbag mechanisms has been indicated, with the suggestion that inclusion of higher twist effects will introduce the necessary proton helicity flip contributions in order to better account for available data.

2.5 Regge Exchange Mechanism

When s, $-t$, and $-u$ are not sufficiently large, then the factorization into hard and soft process may not apply, in which case neither the pQCD nor the handbag approach is valid. An alternative approach has been proposed by Laget [11] based on Vector Meson Dominance (VMD). In the VMD approach, the photon fluctuates into a vector meson, which

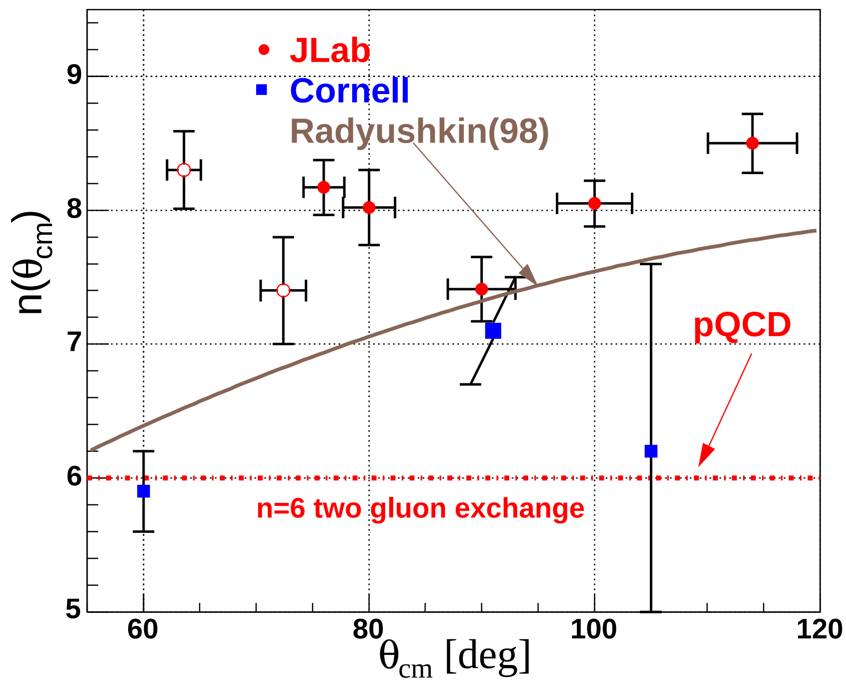

Figure 4: Scaling of the RCS cross sections at fixed θ_{cm}. The open and closed circles are from E99-114. The squares are from the Cornell experiment [30]. The data from E99-114 are consistent with an angle-independent value of $n = 8$, which is inconsistent with the pQCD prediction and the constituent counting rule. The curve is a prediction from Radyushkin based on the handbag model [1].

then interacts with the target via t-channel exchange of mesons (which dominates at low t or forward angles) or u-channel exchange of baryons (which dominates at low u or backward angles). The open question is how high t or u must be in order that the VMD mechanism becomes small compared to the handbag mechanism. The VMD model has had recent successes even at moderately large t. For example the VMD model is able to fit the observed low value of the G_E^p form factor [22] at -t = 5.6 (GeV/c)^2 [31].

Real and Virtual Compton Scattering were studied in a model based on Regge trajectories and two-gluon exchange by F. Cano and J.-M. Laget [11]. The parameters of the model were "tuned" by fitting data from vector meson photoproduction [32, 33], giving rise to predictions for the cross section and spin observables in RCS involving only a single free parameter, the radiative decay constant of the ρ meson. Given the close agreement over much of the kinematic range between the handbag and VMD predictions, they point out that at presently accessible momentum transfer, the contribution to RCS from the hadronic component of the photon is not negligible (see review [34]). Predictions for K_{LL}, K_{LT} and

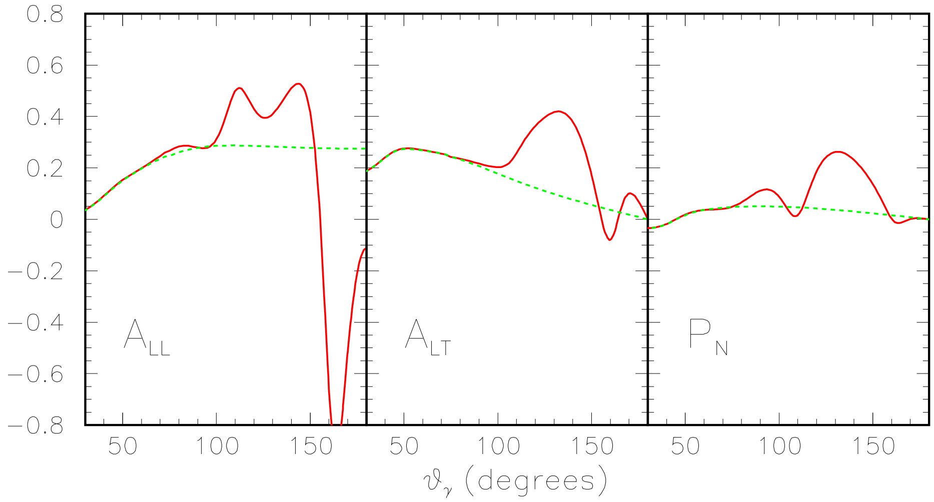

Figure 5: Regge exchange mechanism predictions for RCS polarization observables [11]. The red lines include contributions from u-channel baryon exchange, the green lines do not. $A_{LL} = K_{LL}$ and $A_{LT} = K_{LT}$ for these predictions.

P_N are shown in Fig. 5. The predicted longitudinal polarization transfer K_{LL} is positive, close to the prediction of the handbag approach at θ_p^{cm} below 140°, and close to the result from E99-114. The dominant contribution to K_{LL} in this angular range comes from interference terms between σ-exchange and π-exchange. However, it strongly deviates from the handbag prediction at larger angles, where the u-channel exchange of baryons becomes dominant. Both K_{LT} and P_N are predicted to be small but positive for both of the proposed kinematic points.

2.6 Additional Remarks

It is important to realize that the issues posed at the start of this section are not limited to the RCS reaction. Indeed, they are questions that need to be addressed by all studies of the proton using exclusive reactions in the hard scattering regime. The old paradigm for addressing these questions was the pQCD mechanism and the distribution amplitudes. It is quite feasible that the new paradigm could be the handbag mechanism and GPD's. In any case, the reaction mechanism needs to be tested, not only over a wide range of kinematic variables but also over a wide range of different reactions. Of these, RCS offers the best possibility to test the mechanism free of complications from additional hadrons.

It is also important to realize that any evidence for non-zero K_{LT} and P_N is evidence for hadron helicity flip. Such evidence has already been seen in the G_E^p/G_M^p experiment, as discussed above. Independent of whether the handbag formalism is the correct one, it is quite likely that there is a very close relationship between K_{LT}/K_{LL} and F_2/F_1, and it is important to learn more about the nature of that relationship.

2.7 Summary of Physics Goals

We propose measurements of the spin observables K_{LL}, K_{LT}, and P_N at an incident photon energy of 4.3 GeV (s=8.95 (GeV/c)^2) at two different scattering angles corresponding to $-t$ values of 3.64 and 4.88 (GeV/c)^2. The specific physics goals are as follows:

1. Provide a stringent test of the notion that the RCS reaction proceeds via the interaction of the photons with a single quark.

2. Measure the ratio K_{LT}/K_{LL} and compare with the corresponding values of F_2/F_1 determined from elastic electron scattering in order to identify the role of hadron helicity flip in this reaction.

3. Measure P_N in order to aid in the further development of the theoretical framework.

The overall statistical precision with which we will address these physics goals will be discussed in Sec. 5.

3 Experimental Setup

The proposed experiment will study the scattering of polarized photons from a liquid hydrogen target, illustrated in Fig. 6. The scattered photon will be detected in the BigCal calorimeter installed at a distance to match the acceptance of the HRS-left, which will be used to detect the recoiling proton.

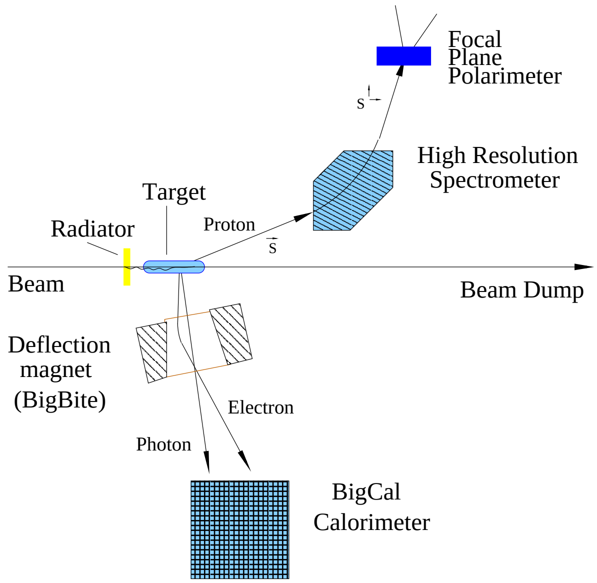

Figure 6: The experimental setup.

3.1 The CEBAF Polarized Beam

Based on our experience with E99-114, we assume an incident electron beam of intensity up to 80 μA in Hall A and with 80% polarization. Such currents and polarizations have already been delivered over long periods of time using the strained GaAs source at Jefferson Lab. The beam polarization will be measured to a systematic uncertainty of 3% with the Møller polarimeter. The large cross section and helicity asymmetry for π° photoproduction, as determined from E99-114, will allow for a continuous check of the product of the electron beam polarization and FPP analysing power during data taking at fixed kinematic conditions. Continuous monitoring of the beam polarization can also be done using the Compton polarimeter.

3.2 The Liquid Hydrogen Target and the Radiator

The experiment will utilize the standard Hall A liquid hydrogen (LH2) target with a 15-cm long machined cell, which was successfully employed in many experiments in JLab.

The radiator will be mounted on the cell block about 4 inches upstream of the cell entrance window. The short distance between the target and radiator helps to avoid background produced from Al walls of the target.

3.3 The Deflection Magnet

It was shown in the E99-114 experiment that the deflection magnet provides sufficient separation of electron and photon elastic scattering events (see Fig. 7). The magnet obviates the need for a veto detector, which in turn allows us to utilize at least ten times higher photon intensity. The deflection magnet for the proposed experiment will be the BigBite magnet which, because of a larger field integral, will offer even better separation than the one constructed for and used in E99-114 (see Fig. 8).

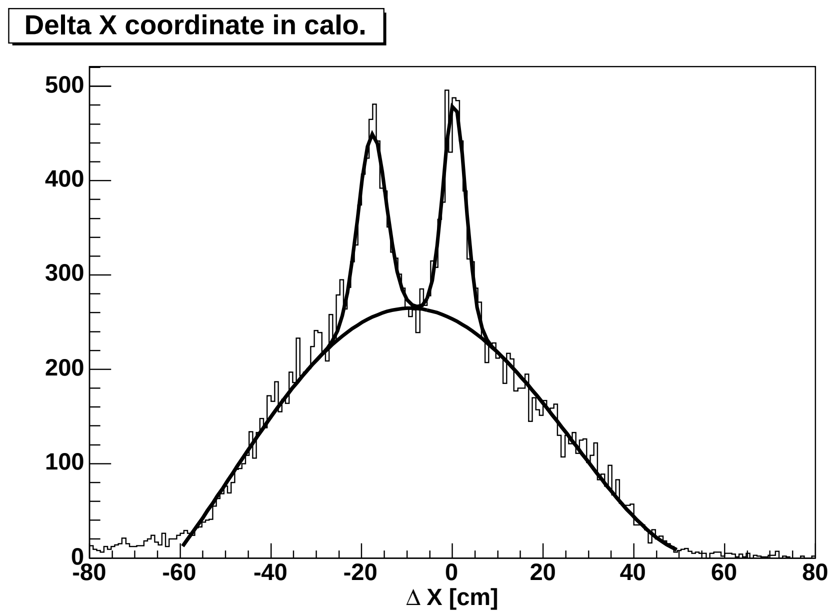

Figure 7: Experimental data from E99-114 at the kinematics $E = 4.3\,GeV$ and $\theta_\gamma^{lab}= 57^o$ showing the event distribution in the horizontal plane. The peak at coordinate ΔX = 0 corresponds to the RCS events. The peak at ΔX = -18 cm corresponds to the elastic electron scattering, which is offset from the RCS peak due to the deflection magnet.

3.4 The Photon Calorimeter

We have participated in the construction and installation of the BigCal calorimeter for the GEP-III experiment in Hall C [35]. This calorimeter consists of 1750 lead glass blocks of type TF-1. There are 32 columns and 56 rows of blocks. Figure 20 shows the front and

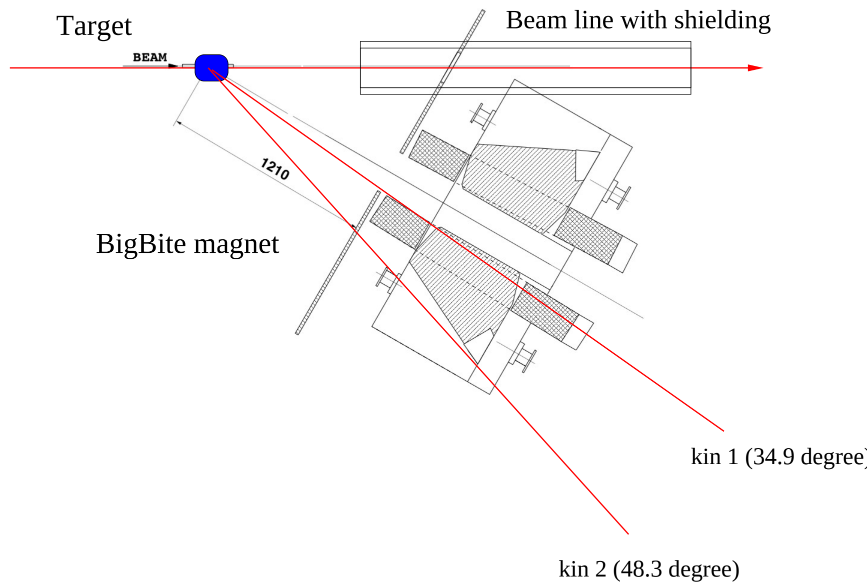

Figure 8: Layout of the deflection magnet (BigBite is shown at angle 30^o as it will be used during experiment E06-010. The red lines indicate orientations of the magnet midplane for proposed kinematics P2 and P3.

top view of the calorimeter and support structure and the front end electronics. It can be moved into the hall without disconnecting the calorimeter from the front end electronics.

The position of the photon arm will be adjusted for each kinematics to match the HRS. As was successfully realized in E99-114, the movement of the calorimeter will be achieved by using the overhead crane and manual pulling of the cable train. Less than two hours (beam off to beam on) was used in a typical access into the hall for movement of the calorimeter.

3.5 The Data Analysis Procedure

We describe below the simplified version of the analysis procedure. The correlation between expected and observed positions of the photon on the front face of calorimeter is the primary parameter used in analysis of the RCS experiment. The expected photon position is calculated from the measured value of the proton momentum, its direction and position at the target. An example of such kinematical correlation from E99-114 is shown in Fig. 9. Three types of events are present: RCS events, which are concentrated at the center ΔX = ΔY = 0; the photopion events, which have wider distribution in both directions ΔX and ΔY; and the electron scattering events, which are peaked at ΔX = - 22 cm, ΔY = 0. The events in the region of $\pm 2\sigma$ around the Compton peak are called the correlated events. and the number of events is N_{corr}. The pion event sample can be made with events located above $\Delta Y = 2\sigma_y$ and below the $\Delta Y = -2\sigma_y$ or with events which have $\Delta X > 2\sigma_x$. Figure 10 shows the ΔY-distribution for events with $-2\sigma_x < \Delta X < 2\sigma_x$ when the shape of pion sample is

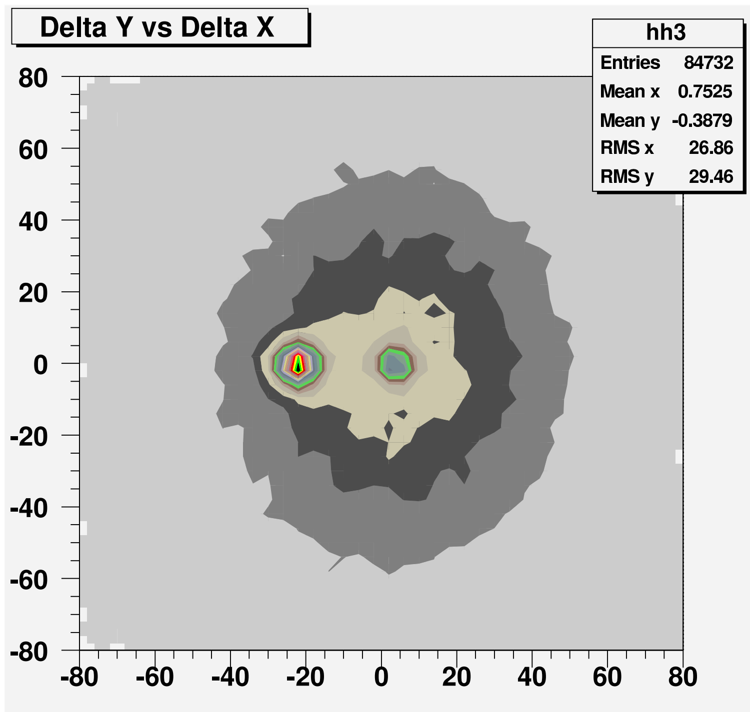

Figure 9: Experimental data from E99-114 at the kinematics $E = 3.23\,GeV$ and θ_p^{cm}=98^o showing the event distribution in the $\Delta X - \Delta Y$ plane.

taken from $\Delta X > 2\sigma_x$.

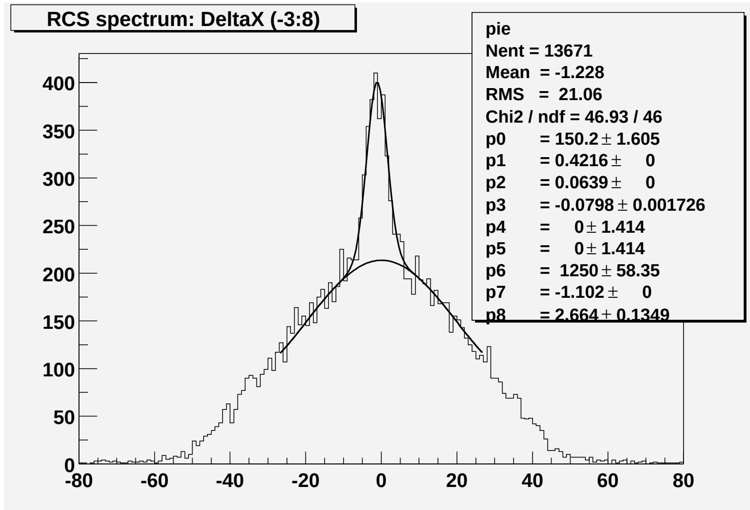

Figure 10: Experimental data from E99-114 at the kinematics $E = 3.23\,GeV$ and θ_p^{cm}=98^o showing the event distribution in ΔY for the cut $-3 < \Delta X < 8$.

3.6 The Focal Plane Polarimeter

The polarization of the recoil proton is measured in the focal plane polarimeter (FPP). Figure 11 shows layout of the FPP with two analyzers, as used in E99-114. Figure 12 shows the notation of the components of the proton polarization at the target. They are P_l (longitudinal), P_t (tranvserse, in the reaction plane), and P_n (normal to the reaction plane). The first two are dependent on the beam helicity, whereas the last is independent. The polarization at the FPP can be found in first approximation (assuming that the HRS is a simple dipole) from expressions

$$P_t^{fpp} = P_t, \qquad P_l^{fpp} = P_l \cdot \cos\chi - P_n \cdot \sin\chi$$
$$\text{and} \qquad P_n^{fpp} = P_l \cdot \sin\chi + P_n \cdot \cos\chi$$

where χ is the spin precession angle relative to the direction of the momentum given by $\chi = 86^\circ \cdot E_p$ (GeV) $[\theta_{bend}/45^\circ]$. For example, for a proton with momentum 3.0 GeV/c the average precession angle in the HRS is 270°, so the longitudinal component of the proton polarization alone defines the value of the P_n^{fpp}. The P_n^{fpp} has a helicity dependent part $P_{n,h}^{fpp}$ related to P_l and a helicity independent one related to P_n.

Figure 13 demonstrates the principles of operation of the FPP. The method is based on the scattering of the proton from the analyzer material. The number of protons which scatter from the analyzer can be expressed as a function of their polar and azimuthal angles, θ and ϕ, respectively, as

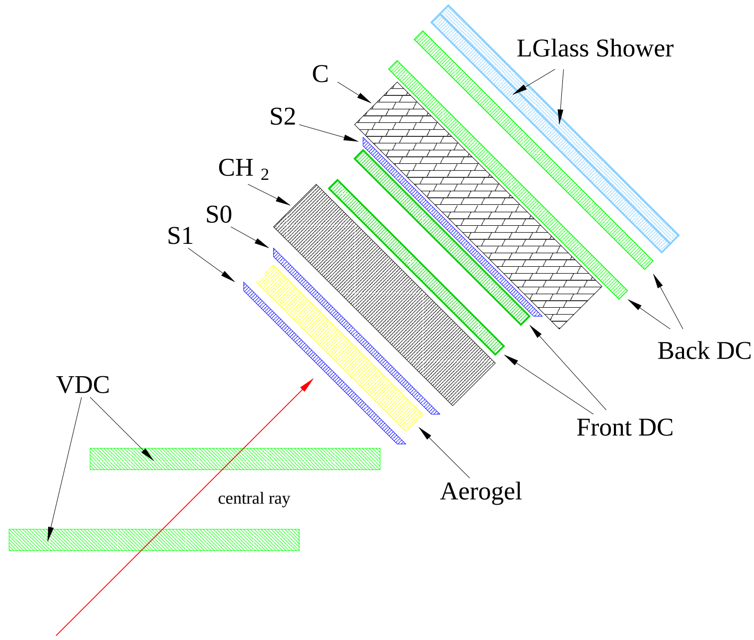

Figure 11: The structure of the detector package in the HRS with the focal plane polarimeter. The vertical drift chamber (VDC), the front drift chambers and back drift chambers are used in FPP tracking analysis. The aerogel Cherenkov counter is used for pion rejection.

$$N(\phi,\theta) \;=\; N_p(\theta)\left[1 \,+\, h\cdot A_y(\theta)\cdot(P_t^{fpp}\cdot\sin\phi \,-\, P_{n,h}^{fpp}\cdot\cos\phi) \,+\, A_y(\theta)\cdot(P_n^{fpp} - P_{n,h}^{fpp})\cos\phi\right]$$

where $h = \pm$ is the sign of the beam helicity; $A_y(\theta)$ is the analyzing power, which is an empirical function of θ, the proton momentum, and structure of the analyzer material; and the N_p^h is the total number of protons incident on the polarimeter. The FPP allows a determination of the two components of the polarization perpendicular to the proton momentum in the focal plane - P_t^{fpp} and P_n^{fpp}. Since the normal component of the proton polarization P_n is helicity-independent, all three polarization components at the target can be determined as

$$P_n \;=\; (P_n^{fpp} - P_{n,h}^{fpp})/\cos\chi, \quad P_l \;=\; P_{n,h}^{fpp}/\sin\chi, \quad P_t \;=\; P_t^{fpp}$$

3.6.1 Figure-of-Merit of the Focal Plane Polarimeter

The statistical accuracy of the polarization measurement δP is expressed as

$$\delta P \;=\; \sqrt{2/\left[\epsilon A_y^2\cdot(N_p^+ + N_p^-)\right]}\,,$$

where ϵ (the FPP efficiency) is the fraction of incident protons with scattering angle θ in the range of large analyzing power; A_y is the average analyzing power over the same range of

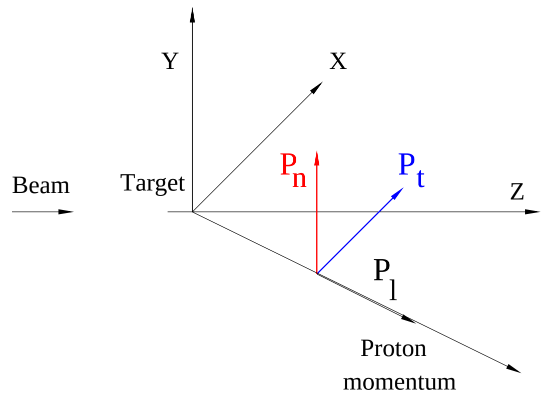

Figure 12: The definition of the polarization components at the target.

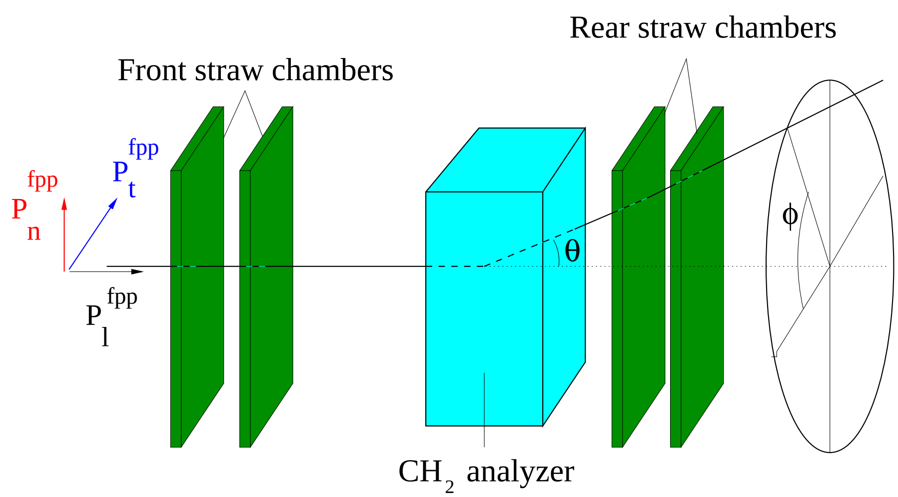

Figure 13: The operation of the Focal Plane Polarimeter.

scattering angles; and $N_p^{\pm}$ is the number of incident protons for each photon helicity. The Figure-of-Merit (FOM), ϵA_y^2, as well as total events $(N_p^+ + N_p^-)$, determine the statistical accuracy of the asymmetry measurement. The analyzing power depends on the proton momentum and polarimeter structure (see for example reference [36]). It is a function of the transverse component of the proton momentum after the scattering $p_{trans} = p_p \sin\theta$. The two most common materials used as an analyzer are Carbon and Polyethylene (CH_2). The FOM for CH_2 is 1.25 larger than that of Carbon [37]. Moreover the maximum A_y is always located at $p_{trans} \sim 0.30$ GeV/c. For optimized thickness of the analyzer, the value of the maximum was described by $A_y = 0.40/p_p$ (GeV/c) for CH_2 analyzer [37].

According to the analysis of the double-analyzer FPP configuration used in E99-114, the total FOM was the sum of 0.0013 for the CH_2 (thickness = 44 cm) and 0.0006 for the Carbon analyzer (thickness = 60 cm) at $p_p = 3.0$ GeV/c. These considerations lead to the total FOM of $0.020/p_p^2$ (GeV/c)^2 for two CH_2 analyzers, which we use here for estimates of the required statistics and beamtime.

3.6.2 Calibration of the Proton Polarization

Because the analyzing power is quite sensitive to the polarimeter structure, the practical way to determine the analyzing power is a calibration of the FPP using the recoil protons from elastic scattering of the polarized electrons. Calibrations allow a measure of both the analyzing power and the instrumental asymmetry. In elastic electron scattering the polarization of the recoil proton at the target can be calculated from the following expressions [38, 39]:

$$P_{t,ep} = -\frac{2\sqrt{\tau(1+\tau)}\,tan\frac{\theta}{2}}{g^2+\tau\epsilon^{-1}} \cdot g \qquad \text{and} \qquad P_{l,ep} = \frac{2\sqrt{\tau(1+\tau)}\,tan\frac{\theta}{2}}{g^2+\tau\epsilon^{-1}} \cdot \frac{(E_i+E_f)tan\frac{\theta}{2}}{2M_p}$$

where M_p is the proton mass, $E_{i(f)}$ is the initial (final) electron energy, $g = G_E^p/G_M^p$ is the ratio of the proton form factors, $\tau = Q^2/4M_p^2$ with $-Q^2 = 4E_iE_f\sin^2\frac{\theta}{2}$, and $\epsilon^{-1} = 1 + 2(1+\tau)\tan^2\frac{\theta}{2}$. The values of $P_{t,ep}$ and $P_{l,ep}$ determine the $P_{t,ep}^{fpp}$ and $P_{n,ep}^{fpp}$ used for the calibration process. The beamtime required for FPP calibration with 5% accuracy was between 2 and 10% of that RCS data-taking time.

3.6.3 Analysis of the Helicity Asymmetry in E99-114

E99-114 collected data with polarized photons for the average photon energy of 3.23 GeV and θ_p^{cm} =122°. Figure 14 shows the helicity asymmetry A_h observed in the distribution of recoil protons vs. azimuthal angle in the FPP for elastic electron scattering from the proton. A_h was calculated as

$$A_h(\phi) = \frac{1}{2}\left[\frac{N^+(\phi)}{N_p^+} - \frac{N^-(\phi)}{N_p^-}\right],$$

where $N^{\pm}(\phi)$ is an integral of $N^{\pm}(\phi,\theta)$ over the range $\theta = 3° - 20°$. The observed asymmetries for both analyzers are about 0.053. These results were used for calibration of the FPP.

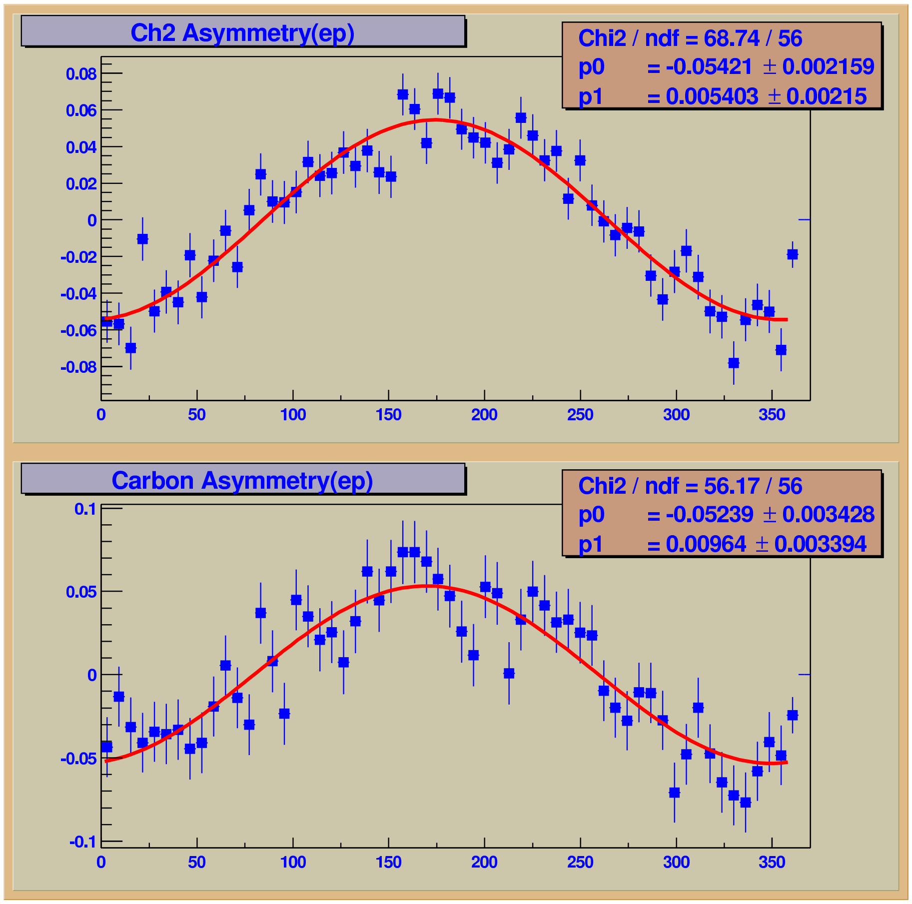

Figure 14: Beam helicity asymmetry for elastic electron scattering from proton.

Figure 15 shows the helicity asymmetry for the π° photoproduction. Figure 16 shows the asymmetry for the kinematically correlated events, where RCS and π° events are mixed in ratio of 1:2. The asymmetries obtained from the above analysis are A_{ep}, A_{π°, and A_{corr} (we droped helicity index h in expressions here and below). Each of them has two components, A_t and A_n, denoted on the plots as $P0$ and $P1$, respectively.

The asymmetry for RCS events is determined from the following:

$$A_{_{RCS}} = A_{corr} \cdot D - A_{\pi^\circ} \cdot (D-1)$$

where D is a dilution factor defined as $(N_{\gamma,\pi^\circ} + N_{\gamma,\gamma})/N_{\gamma,\gamma}$ for the kinematically correlated photon-proton events. Because of the large number of π° events, A_{π° is very well determined so that the accuracy of $A_{_{RCS}}$ is determined by the statistical precision of A_{corr}:

$$\delta A_{_{RCS}} = D \cdot \sqrt{2/N_{corr}}$$

The P_t and P_n components of the proton polarization at the FPP for RCS are expressed as

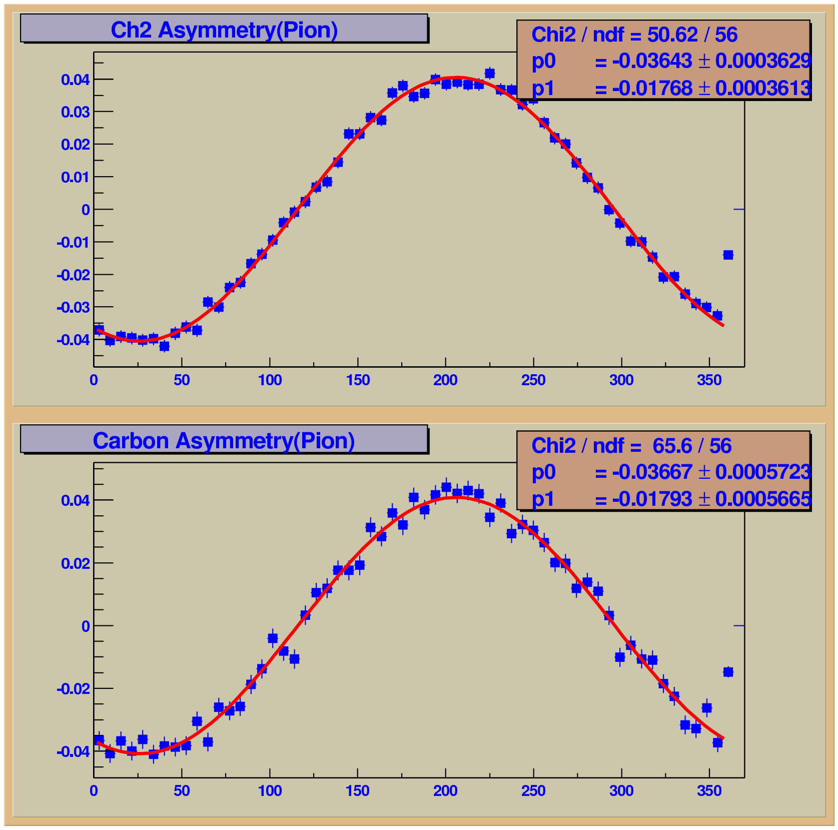

Figure 15: Beam helicity asymmetry for the π° photoproduction from proton.

$$P^{fpp}_{t,RCS} = P^{fpp}_{t,ep} \cdot \left[P0_{corr} \cdot D - P0_{\pi^\circ} \cdot (D-1)\right] / P0_{ep}$$

$$P^{fpp}_{n,RCS} = P^{fpp}_{t,ep} \cdot \left[P1_{corr} \cdot D - P1_{\pi^\circ} \cdot (D-1)\right] / P0_{ep} \,.$$

In the last formula we used the $P0$ component of the asymmetry and $P^{fpp}_{t,ep}$ because it is better determined than $P1$ for the kinematics of our experiment. These formulas determine the magnitude and direction of the proton spin at the FPP in the proton rest frame relative to the direction of the proton momentum in the lab frame.

The preliminary results of E99-114 (averaged from both analyzers and normalized to 100% photon polarization) are

$$P_{l,RCS} = 0.75 \pm 0.11 \quad P_{t,RCS} = -0.10 \pm 0.10$$

3.6.4 Transformation to the CM Frame

The FPP is calibrated based on the polarization of the proton from elastic electron scattering, whose components were calculated relative to the direction of the proton momentum

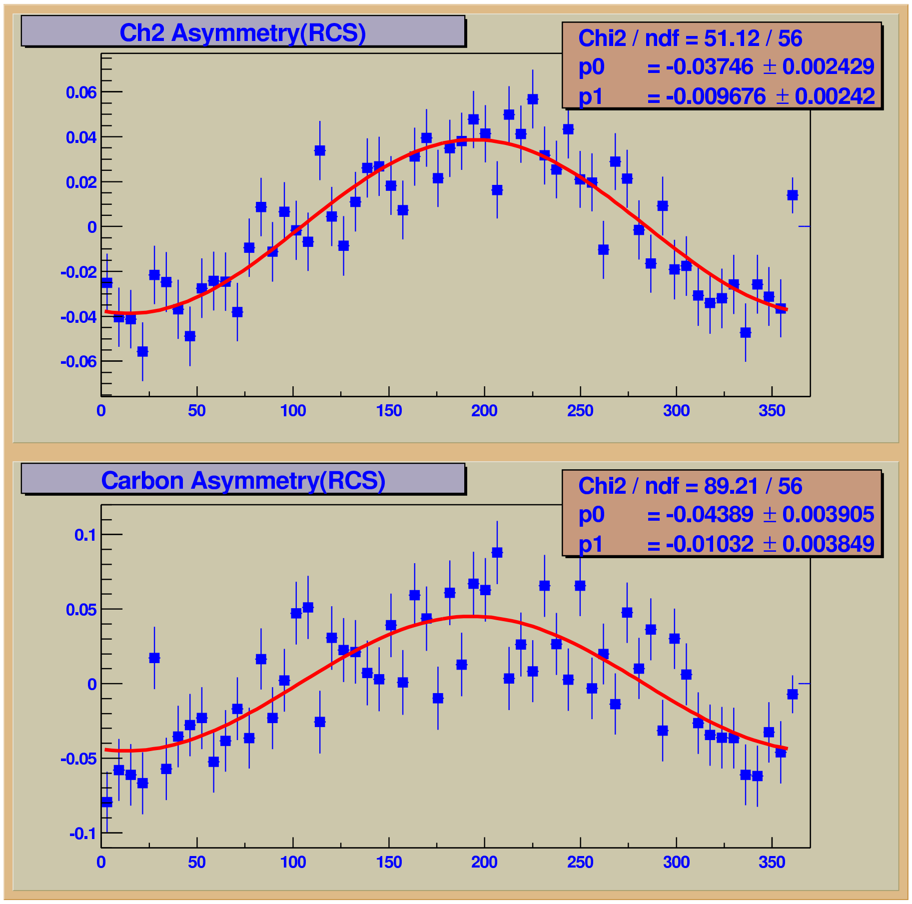

Figure 16: Beam helicity asymmetry for kinematically correlated photon-proton events.

in the lab frame. Therefore the results for RCS are found also relative to the direction of the the proton momentum in the lab frame. The calculations of RCS polarization observables done in the photon-proton cm frame, so the observed experimental proton polarization need to be transfered also to photon-proton cm frame.

The transformation from lab to cm frame can be represented as a rotation of the polarization vector by angle α. The magnitude of the proton polarization is unchanged in the transformation, but the values of the l and t components are changed as follows:

$$
\begin{aligned}
P^{cm}_{l,RCS} &= P^{lab}_{l,RCS} \cdot \cos\alpha - P^{lab}_{t,RCS} \cdot \sin\alpha \\
P^{cm}_{t,RCS} &= P^{lab}_{l,RCS} \cdot \sin\alpha + P^{lab}_{t,RCS} \cdot \cos\alpha
\end{aligned}
$$

For the kinematics of E99-114 polarization measurements, $\alpha = 20^\circ$ which leads to polarization transfer parameters $K_{LL} = 0.74 \pm 0.11, \quad K_{LT} = 0.16 \pm 0.11$.

4 Proposed Measurements

A longitudinally polarized electron beam of energy 4.8 GeV with current of 80 μA will be used for both kinematic points. The Cu radiator with thickness of 1.3 mm (10% radiation length) will be installed 4 inches upstream of the 15 cm-long liquid hydrogen target. Photons of average energy 89% of the electron beam energy will be used. For such bremsstrahlung photons, the circular polarization is almost equal polarization of the electrons. The recoil proton will be detected in the HRS-left magnetic spectrometer. The scattered photon will be detected in the large calorimeter BigCal. The components of the polarization of the recoil proton will be measured in the focal plane polarimeter (FPP).

All features of the experimental technique were used in E99-114. The larger size of the BigCal calorimeter will allow the experiment to be done with a larger distance between the target and the calorimeter and consequently a larger luminosity by a factor of 2.5 to be used with the same radiation load per lead-glass module. Analysis of the trigger rate and signal amplitude fluctuation due to high rate effect in E99-114 data show that load per block could be **doubled** with no loss of performance for RCS events.

4.1 The Kinematics

The central momentum of the proton spectrometer will correspond to the elastic scattering of the photon (or electron) with initial energy 4.3 GeV (about 11% below the beam energy). The overlap of the acceptances of the photon and proton arms will be done the same way as in E99-114, with the photon arm having the defining angular acceptance. Figure 17 shows the simulation of the incident photon spectra folded with the combined acceptances of the two arms. The effective photon energy range, which we are going to use in analysis, defined also by the acceptance overlap, is approximately 0.4 GeV or 10% of incident photon energy. The proposed measurements are presented in Table 1, where α is the spin rotation angle for transformation from the laboratory to cm frame.

kin. P#	t, $(\text{GeV}/c)^2$	u, $(\text{GeV}/c)^2$	θ_γ^{lab}, degree	θ_p^{cm}, degree	θ_p^{lab}, degree	E_γ^{lab}, GeV	p_p GeV/c	precession χ, degree	sinχ	α, degree
P1	-3.64	3.55	34.9	90	30	2.36	2.72	247	-0.92	29.7
P2	-4.88	2.31	48.3	110	22	1.70	3.41	304	-0.83	21.9

Table 1: The kinematics parameters of the proposed measurements at $s = 8.95$ $(\text{GeV}/c)^2$.

4.2 Expected Rates

In E99-114 unpolarized data were collected for the average photon energy of 4.3 GeV and θ_p^{cm} in range $70° - 110°$. Table 3 presents the cross section of RCS process at photon energy of 4.3 GeV. The event rates are the products of the luminosity, the cross section, and the

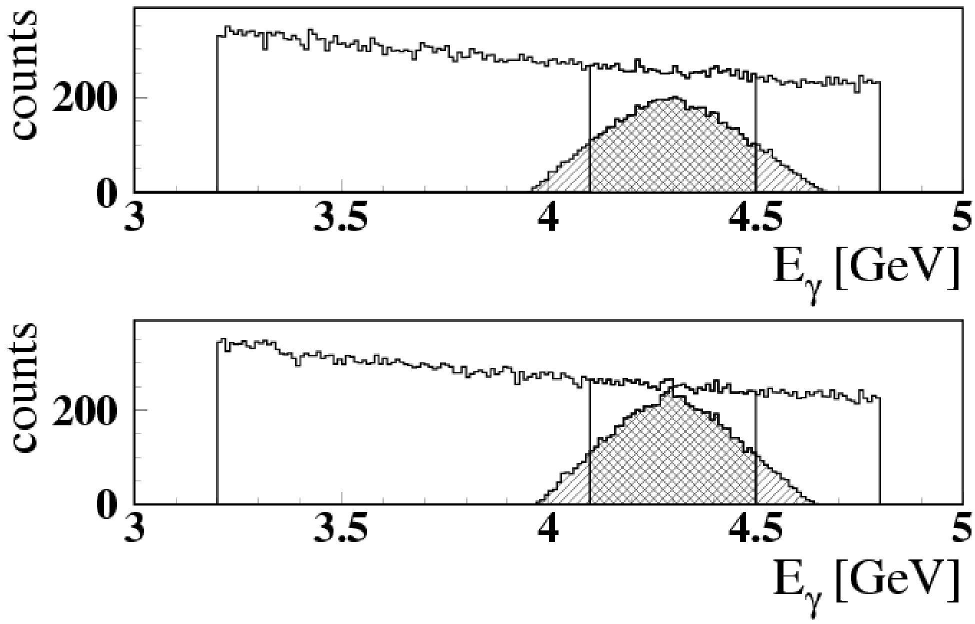

Figure 17: The simulated photon spectra for the proposed kinematics P1, P2 (from the top to the bottom). The photon spectra in coincidence with the proton are shown by dashed area.

acceptances of the detectors, as well all other factors such as DAQ dead time, efficiency of the trigger and the detectors, efficiency of the reconstruction analysis. The rate, N_{RCS} was calculated as:

$$N_{RCS} = \frac{d\sigma}{dt}_{RCS} \frac{(E^f_\gamma)^2}{\pi} \Delta\Omega_\gamma f_{\gamma p} (\frac{\Delta E^f_\gamma}{E^f_\gamma} \frac{t_{rad}}{X_o}) \mathcal{L}_{ep}$$

where $\frac{d\sigma}{dt}_{RCS}$ is the RCS cross section (see Table 2); the factor $\frac{(E^f_\gamma)^2}{\pi}\Delta\Omega_\gamma$ is the range of Δt for the given kinematics, expressed through the energy of the scattered photon and the solid angle of the photon detector; $f_{\gamma p} = 0.4 - 0.7$ is the fraction of events detected for given range of photon energy E^f_γ; $(\frac{\Delta E^f_\gamma}{E^f_\gamma} \frac{t_{rad}}{X_o}) = 0.4/4.3 \cdot 0.13$ is the number of photons per incident electron, including the photons produced in the target and virtual photons; $\mathcal{L}_{ep} = 2.9 \cdot 10^{38}$ cm^{-2}sec^{-1} is the electron-proton luminosity for 80 μA beam. The simulated photon spectra for the proposed kinematics is shown in Figure 17.

The Table 2 also shows the dilution factor D defined as $(N_{\gamma,\pi^\circ} + N_{\gamma,\gamma})/N_{\gamma,\gamma}$ for the kinematically correlated photon-proton events and the $f_{\gamma p}$, the phase space factor for the proton arm. The observed calorimeter rate was used to choose experiment luminosity. The observed cross section was used for an estimate of the rates in the proposed experiment. We extrapolate the cross section linearly between data points inside the angular region of E99-114. Table 3 presents main parameters of kinematics and the expected RCS events rates for

kin. 4#	θ_γ^{lab} degree	-t, $(\mathrm{GeV}/c)^2$	θ_p^{cm}, degree	D	$F_{trigger}$ kHz/msr/μA	$d\sigma/dt$ pb/$(\mathrm{GeV}/c)^2$
4A	22	2.03	63.8	2.13	0.80	456
4B	26	2.57	72.8	1.54	0.53	146
4C	30	3.09	81.1	1.67	0.56	78
4D	35	3.68	90.4	2.75	0.40	40
4E	42	4.39	101.5	2.80	0.51	30
4F	50	5.04	112.1	2.42	0.62	36
4G	57	5.48	119.9	2.83	0.42	54
4H	66	5.93	128.4	3.89	0.30	65

Table 2: The cross section of RCS for 4.3 GeV photon energy. Here D is dilution factor. $F_{trigger}$ is the calorimeter trigger rate at the threshold of 55% of the RCS photon signal.

a range of kinematics around the proposed measurements. The distance between the target and the calorimeter was optimized to match the acceptance of the proton spectrometer. The resulting solid angle of the photon arm $\Delta\Omega_\gamma^{lab}$ and acceptance factor $f_{\gamma p}$ are shown in the same table.

kin. P#	θ_γ^{lab}, degree	$\Delta\Omega_\gamma^{lab}$, msr	t, $(\mathrm{GeV}/c)^2$	θ_p^{cm}, degree	Dist, m	$f_{\gamma p}$	$\nu_{_{RCS}}$ Hz
P1	34.9	9.8	3.64	90	15	0.62	2.
P2	48.3	21.8	4.88	110	10	0.71	2.2

Table 3: The expected rates of RCS events in the proposed experiment.

4.3 Required Statistics

As was shown in Sec. 3, the Figure-of-Merit of the FPP is approximately $\sim 0.020/p_p^2$ $(\mathrm{GeV}/c)^{-2}$. The statistics required for obtaining accuracy of $\Delta P_{n,h}^{fpp}$ with 80% photon beam polarization (which is included in determination of the FOM) can be calculated:

$$N_{_{RCS},required} = 100 \cdot p_p^2 \cdot D/sin^2\chi/(\Delta P_{n,h}^{fpp})^2\,.$$

Table 4 presents required statistics for each kinematics. The larger uncertainty in $P_{_N}$ is related to less favourable spin transport through the HRS-left.

4.4 Systematic Uncertainties

The overwhelming contribution to the overall systematic uncertainty associated with the proposed recoil polarization measurements comes from how precisely one knows the dilution factor for the background photopion events. In the case of the polarization analysis in E99-114, this factor was obtained from a fit to the background continium, as in Fig. 10. However,

kinematic	P1	P2
N_{RCS}, events	0.98M	1.7M
ΔK_{LL}	0.05	0.06
ΔP_N	0.13	0.09
ΔK_{LT}	0.05	0.05

Table 4: The statistics and expected statistical accuracy in the proposed experiment. The values of the uncertainties were not adjusted for spin rotation in the transformation between the laboratory and cm systems.

during the E99-114 cross section analysis a dedicated Monte Carlo calculation was developed in order to provide a better account of the background shape. This same Monte Carlo will be employed during analysis of the proposed measurement. Based on a comparison of these two techniques an improvement by a factor of 1.5 to 2 in the overall systematic uncertainty is expected.

5 Expected Results and Beam Time Request

5.1 Expected Results

The purpose of this experiment is to measure the polarization transfer parameters K_{LL}, K_{LT}, and P_N with accuracy sufficient to obtain conclusive evidence on the dominance of the specific reaction mechanism for the RCS process in the several GeV energy range. Figure 18 shows the expected results and different predictions for the longitudinal polarization transfer K_{LL}.

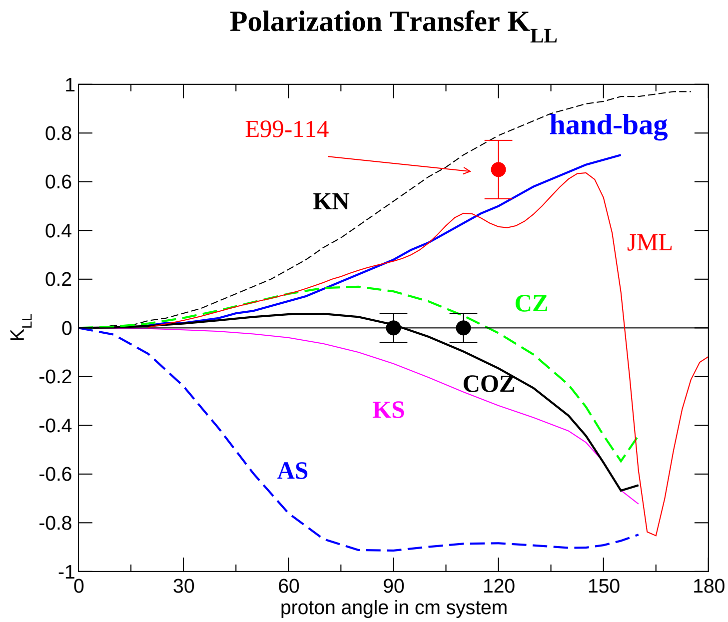

Figure 18: Polarization transfer observable K_{LL} in the RCS process with expected statistical accuracy of the proposed measurements shown as black circles. The labels on the curves are KN for the asymmetry in the hard sub process; the pQCD calculations [7] with AS for asymptotic distribution amplitudes, with CZ for Chernyak-Zhitnitsky [41], with COZ for Chernyak-Ogloblin-Zhitnitsky [42], with KS for King-Sachrajda [43]; hand-bag for calculations in Soft overlap approach [3], JML for calculation in Regge approach [11].

Other experimental observables (K_{LT} and P_N) also could be directly compared with predictions of GPD-based theory (see Sec. 2.2 and Ref. [3]) and with predictions of non-GPD models [17],[18] (see e.g. Fig. 19). We propose to obtain the statistical accuracies shown in Table 4, which will lead to the expected results for K_{LL} that are shown in Fig. 18. Systematic uncertainties are expected to be around half of the statistical uncertainties.

5.2 Beam Time Request

The proposed experiment will be done at one beam energy of 4.8 GeV with current up to 80 μA. In order to achieve the results discussed above, we **request beam time of 21 days in Hall A** as it is summarized in Table 5.

kin. P#	procedure	beam, μA	time, hours	charge Coulomb
P1a	Beam pol. measurement	1	8	
P1b	FPP calibration	80	8	2
P1c	BigCal angle change		4	
P1d	RSC data taking	80	170	49
P2a	BigCal angle change		4	
P2b	FPP calibration	80	30	9
P2c	BigCal angle change		4	
P2d	RCS data taking	80	280	81
total			508	141

Table 5: The beam time request for this experiment.

6 TACs Comments, PACs Questions, and PAC29 Review Report

6.1 Comment from TAC23 and our Reply

Running up to 100 μA on a 6% radiator will cause a high radiation dose at the site boundary.

The first RCS experiment E99-114 used a beam current up to 40 μA on a 6% radiator. The beam energy was exactly the same as in the proposed measurement. This provides exact information on the expected radiation dose integral. Below is the recommendation from P. Degterenko of RADCON group regarding the radiation level.

"The max neutron dose rate at RBM-2 position in the end of February was approximately of the order and less than double Average Dose Rate Design Goal which means that if run continuously through the year the accumulated boundary dose would be twice the administrative limit of 10 mrem. Running with 3 times larger current would correspond three times larger dose rate. In a continuous two-month run you would exceed the budget. I do not know yet what other experiments are planned and what run time do you request, but looks like running for 15-30 days like that would be OK from the point of view of boundary dose. You will probably have significant in-hall Be-7 contamination problem if you run such high beam, too. It's not a catastrophe, but a point to think about in advance."

The maxima during the reference period were above the "Average dose rate design goal" by factor of 1.5. The integration period for this plot is about 1 hour, so the dose maxima correspond to the running at average current close to the requested level of 40 μA.

The proposed experiment plans to use 100 μA beam on a 6% radiator during 130 hours for kinematics P4.
This will lead to the dose which will be higher then the "Average dose rate design goal' by a factor of 4. Because of the relatively short duration of the run - 5.5 days - it corresponds to only 6% of the "Average dose rate design goal" for the twelve month period. Three other kinematics together lead to an additional 4% of the "Average dose rate design goal' for the twelve month period. Because during these two running conditions will be the installation or/and removal of the septum magnet, which expected to take at least one week, and the total running time has in average 60% efficiency the "Average dose rate design goal" can be satisfied even in a period of this experiment (pending of the Hall C schedule).

The kinematic P4 was canceled in the present proposal.

6.2 Reply to PAC23 Questions on Proposal P03-003

Q1: Figure 1 shows the sensitivity in K_{LL} to different models of the reaction mechanism. The proposal outlines a significant effort to measure three quantities (K_{LL}, K_{LT}, P_N). What is the model sensitivity in the latter two observables?

A1: We appreciate the question and provide the following information in response:

- In the asymptotic pQCD mechanism, hadron helicity conservation implies both observables K_{LT} and P_N are zero. In the handbag model K_{LL} is related to the tensor form factor and P_N to the gluonic NLO contributions. Sensitivity to the handbag predictions for K_{LL} and K_{LT} are shown in the proposal in Fig. 17.
- The predictions in the Regge model developed by F. Cano and J. M. Laget are shown in Figure 19. They indicate large values of A_{LT} (which is related to K_{LT}) and P_N (up to 0.2–0.4) at $\theta_{cm} \sim 120 - 140°$.

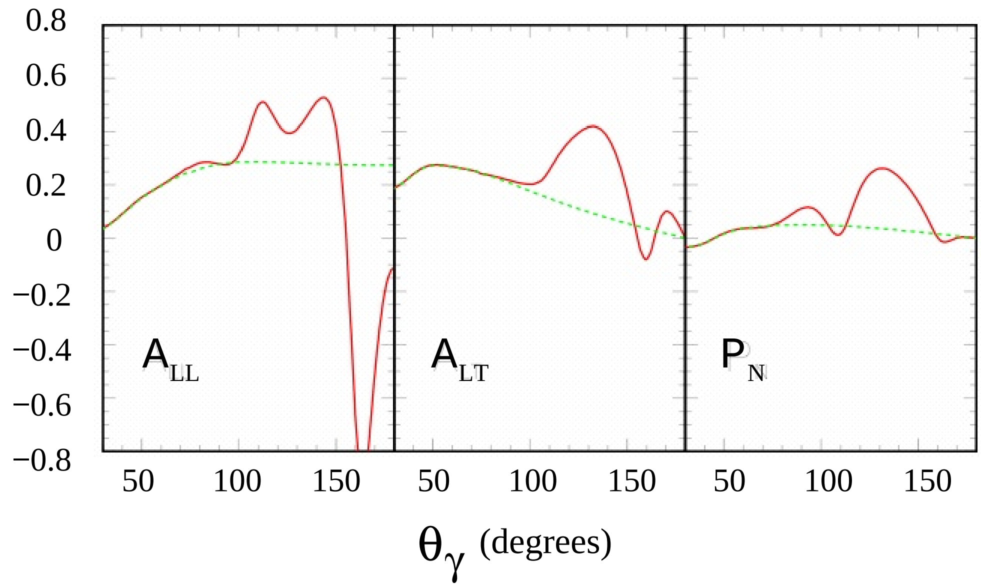

Figure 19: The longitudinal (left), transverse polarization transfer (center) and induced polarization (right) in Compton Scattering at $E_\gamma = 4$ GeV. Solid lines are the final results, which include u-channel exchanges.

Q2: Are there similar sensitivities in other polarization observables? In particular, if similar model sensitivities occurred in beam-target double-polarization asymmetries, these could be measured with much higher efficiency than ones requiring recoil polarization determination. Projected error bars such as those in figure 16 are not bad, but could shrink significantly if one were not fighting the low efficiency of a proton polarimeter, and that would be very appealing.

A2: There are beam-target double-polarization asymmetries A_{LL} and A_{LT}. They are related to K_{LL}, K_{LT} in pQCD as well in the handbag and the Regge models as $A_{LL}= K_{LL}$ and $A_{LT}= - K_{LT}$. The experiment using a polarized target has several advantages. However, when the experiment uses a mixed photon-electron beam and the value of proton momentum is of 3-4 GeV/c, as it is in the present proposal, the Figure-of-Merit for the polarized target is smaller than that of the polarimeter by a factor of 10-20. Moreover, a polarized target would require a clean photon beam line with the electrons dumped upstream of the polarized target. This would require large scale construction and installation efforts. The proposed FPP technique is simply an extension of the technique used in E99-114, which has been shown to work. It is useful to point out, however, that we have considered the polarized target technique in association with the JLab 12 GeV upgrade.

Q3: You propose to use untagged bremsstrahlung from a radiator 4" in front of the target. Some of the detected events should come from p(e,γp)e', or VCS. They will not be as correlated, but since you intend using only the top of the brem spectrum, many could be in the region of interest. How many? Have you simulated this?

A3: There are VCS events expected in our data sample. The fraction of such events were simulated and directly measured during last year E99-114 experiment. It was done during calibration runs without a radiator in front of the hydrogen target. The yield of VCS events is about quarter of the total RCS rate in production run, corresponding to an effective "virtual photon radiator" of 0.02 radiation lengths. It is certainly important to take these events into account for the measurement of the cross section, as has already been successfully done for the deuteron photodisintegration experiments at JLab.

For the proposed polarization experiment, there will also be VCS events in the data sample. We can use the kinematics of the experiment to place reliable upper limits on the virtuality of the incident photon. The photon energy is about 10% below the endpoint, so the electron energy is about 330 MeV. The cut on the kinematical correlation between the recoil proton and the scattered photon is about 5 mrad for both the out-of-plane and the in-plane angles. The energy resolution for the photon is about 3-5%. These numbers lead to upper limits on the electron scattering angle, leading to an upper limit on the four momentum transfer of 0.2 (GeV/c)^2 (according to the data from E99-114). Therefore, these photons are "almost real" so that the Compton scattering of these photons is expected to be governed by the same physics as RCS. For quantitative evaluation of the difference between VCS and RCS observables for low Q^2, we plan to use the calculation developed by M. Vanderhaeghen *et al.*.

Q4: In section 3.6.2 you reserve 10% of the running for calibration from p(e,e'p). Why aren't these events in the data stream, as in figure 5?

A4: There are *ep* events in the data stream. They correspond to electrons with energy below the beam energy by 10%. For these kinematic points, the rate of *ep* events in the data stream is not sufficient for the desired statistical precision on the calibration. Cleaner and faster calibration will be done by using a pure electron beam (without the radiator) and appropriately adjusting the kinematics to get the same recoil momentum. This was exactly the technique use in E99-114.

Q5: You describe your analysis procedure for separating out π events in terms of subtracting spectra with and without the π *dilution*. If the spectra are as clean as in figure 5, why not just fit out the RCS?

A5: It is not possible to obtain data free of pion events. However, it is possible to obtain data free of RCS events, by selecting a different region of the "Delta X - Delta Y" phase space (see proposal Fig. 7), so that accurate numbers can be obtained for the asymmetry of pion events. So, we measure the asymmetry for pure pion events, the asymmetry for mixed RCS-pion events, and the fraction of the latter events that are RCS. The latter number is just the inverse of the so-called dilution factor D and is obtained by fitting spectra such as Fig. 5 in the proposal.

Q6: You plan to use an extended target of 15 cm. This will affect your angle reconstruction? Was the data of figure 5 collected with a target of similar thickness?

A6: The data of figure 5 were collected in the E99-114 experiment with a target of 15 cm and the same wall thickness. The position of the event vertex in the target affects the angle reconstruction. The position was determined for each event by using proton track information in the HRS spectrometer with an accuracy of better than 5 mm.

Q7: In section 6.2 you discuss the radiation damage accumulated in E99-114 after 30 Coulombs. Is it clear that the blocks will last the 87 Coulombs of the current proposal? You discuss curing the damage with UV radiation and estimated that would take 8 shifts. How many such cycles do you estimate will be required? (This is a function of how the degraded resolution hampers the RCS/(e,e') separation.) This doesn't seem to be in your run plan; is it your intention to request that the allocated running time to be broken up into well separated sections? If so, do you need access to the target during these times?

A7: The proposed experiment plans to use a calorimeter with a surface area 2.5 times larger than that of E99-114. It will allow us to increase the distance between the target and the calorimeter, and the intensity of electron beam, by the *same factor* without loss of acceptance. As result the total radiation damage of the lead glass in the proposed experiment will be about the same as it was in experiment E99-114. We plan to do the UV curing procedure only one time, before or after data taking for the kinematics P4. The run plan requires two different configurations of the HRS spectrometer: with and without the septum magnet. The time needed for reconfiguration of the HRS will be several times longer than time needed for the UV curing procedure. That is the reason why the time for UV curing was not discussed in the run plan.

We assume that experiment will be broken into two sections: kinematics P1-P3 and kinematics P4, the latter requiring the septum magnet.

Q8: I'm afraid find the discussion regarding the polarimeter on p.17 a bit confusing. The function $N^h(\phi, \theta)$ describes the response of the FPP but depends on the beam helicity (h) ??? The response of a proton polarimeter ought not to depend on how the protons were generated.

A8: We focused the discussion in the proposal on extraction of the helicity-dependent polarization observables. Use of helicity information allows one to avoid a measurement of the instrumental asymmetry. It is the reason why helicity is so important for the function $N^h(\phi, \theta)$. However, it is true that extraction of $P_{_N}$, which is not helicity dependent, does require knowledge of the instrumental asymmetry. This will be obtained from the *ep* calibration.

Q9: In the discussion preceding eqn.(4) you describe $\sigma_{_{KN}}$ as Klein-Nishina scattering from *a* quark. Although not explicitly evident in eqn.(4), I presume this is summed over all three quarks?

A9: In $\sigma_{_{KN}}$, a unit charge was assumed. The coherent sum over all quark configurations, properly weighted by the square of the quark charge, is absorbed into the form factors (see the formulas on page 8 of the proposal).

6.3 Comments from TAC29 and our Reply

Q1: Running up to 100 A on a 10% radiator will cause a high radiation dose at the site boundary.

R1: The analysis of radiation at the site boundary was addressed in our reply to the TAC23, see Sec. 6.1.

Q2: This proposal requires a large installation effort, both for BigCal the new HMS polarimeter and for BigBite.

R2: The experiment installation time will be minimized by optimization of the schedule. Recent successful installation of the GEN E02-013 experiment, which installation volume was about three times larger than expected in this proposal, allow us to plan **one month** for installation of the BigCal (including DAQ) and BigBite magnet in Hall A.

6.4 Reply to PAC31 on Proposal P07-002

PAC31 report tell the following: **Proposal: PR-07-002**

Scientific Rating: N/A for the Hall A part, B for the Hall C part

Title: Polarization transfer in Wide Angle Compton Scattering

Spokespersons: B. Wojtsekhowski, A. M. Nathan, R. Gilman

Issues: There is consensus in the PAC that the previously published polarization measurements have clearly shown a contradiction with the pQCD predictions. Although this looks quite evident also from measurements of other reactions and observables (e.g. the ratio of the electric to magnetic elastic proton form factors), having some more evidence from the RCS polarization observables may be beneficial. On the other hand, the PAC felt that, given the absence of a rigorous proof of a factorization theorem, the assumption that the reaction proceeds via a handbag diagram involving a current quark seems only weakly justified. The agreement of the data with this particular approach does not seem to be sufficient to conclude that the physics is indeed driven by the GPDs. For instance, an alternative approach based on constituent quarks may equally explain the data. Although in the latter case there would be also an interesting insight into the reaction mechanism, the connection with the GPDs would be lost and so would be much of the exciting physics presented in the proposal. Therefore, given the large effort involved in measuring the polarization observables in RCS at all the proposed angles, but considering the interest in having some additional information on the behavior of these observables in a fundamental exclusive reaction, to be compared with model predictions, the PAC decided to approve only the Hall C measurement, as it has the minimum overhead and beam time impact. For the Hall A part of the proposal instead, the PAC decides for deferral.

Recommendation: Defer in Hall A, Approve for 3 days in Hall C

In response, we like **to agree that previous experiment clearly demonstrated disagreement with pQCD in s-scaling, however K_{LL} measurement was done at relatively low u**, where predictions for K_{LL} made in pQCD mechanism as well as in other approaches may not work. Measurement of K_{LL} looks as a most promising way to learn about reaction mechanism, its value largely independent of theoretical development of the handbag model calculation and proof of handbag factorization. It is important to check the shape of K_{LL} angular dependence at kinematic parameters where predictions are applicable. Test will show to what extent experimental shape is close to calculated one for real Compton scattering on spin 1/2 point like particle.

The results of experiment would stimulate further theoretical efforts in refining the QCD and quark model approaches for understanding the physics of wide-angle RCS on the proton. The proposed measurements are in a kinematic regime where s is larger than previously, and $-t$ and $-u$ are both significantly larger than the proton mass scale. We also agree that more theoretical work is needed in the handbag approach.

Whether through GPD's, proton wave functions based upon CQM, distribution amplitudes or indeed some other parameterization of nucleon structure, we know that RCS is one of the very few unique and fundamental reactions, involving as it does only one hadron, from which more can be learn. Moreover, these theoretical approaches are not mutually exclusive, as we have seen in dualities between CQM and pQCD based models in DVCS and elastic form factor calculations.

The simultaneous measurement of three independent polarization observables will further enhance our understanding of the reaction mechanism and the role of soft physics in this energy regime, primarily, although not exclusively, through the recoil polarization transfer K_{LL}. This observable will continue to be one of the key indicators of the RCS reaction mechanism and the underlying physics as a new kinematic domain opens up before us.

We would also like to add that installation of BigCal was recently completed in Hall C, the time-frame and efforts for which was consistent with our estimate of required time in Hall A of four weeks.

7 Technical Considerations

7.1 The Cryotarget and Radiator

The standard Hall A cryotarget with the machined cells of 15 cm length will be used. This cell type was used with beam current up to 100 μA during recent experiment E99-115. The radiator will be mounted on the cell block as it was done during experiment E99-114.

7.2 The Calorimeter

We plan to use a calorimeter which is currently being used in the experiment E01-109 [35]. Figure 20 shows the layout of the detector. It consists of 1750 blocks in 32 columns and 56 rows. The PMT FEU-83-4 will be used for light detection. This Figure also shows configuration of the calorimeter and front end electronics. The stand, which supports the calorimeter and electronics, can be moved into the hall without disassembling, so installation time is needed only for connecting about two thousand 100 m long cables between the detector and DAQ. Such work will require about 70 man-shifts.

The energy resolution for the calorimeter, obtained at the beginning of the experiment E99-114, was 5.5% (for 1 GeV photon energy). It became 10% at the end of the run as result of radiation effects on lead glass transparency (see Fig. 21). Total accumulated beam charge in the experiment E99-114 was 30 Coulomb. In E99-114 the front face of the lead glass was protected by plastic material with effective thickness of 10 g/cm^2. Because it is found that the experiment can be done without veto counters for proposed measurement we plan to use an Al protection sheet of 5 cm thickness to mitigate the radiation damage of the lead glass.

We had developed and tested on the E99-114 calorimeter the technique of curing of the radiation effects. Irradiation by UV light will be done in situ without disassembling of the lead glass stock. However, it is required to remove all PMTs, because large intensity light can damage the photocathode. The whole process of the calorimeter resolution recovery will take about 8 shifts.

7.3 The Proton Spectrometer

The HRS-left will be used in the proposed experiment. The trigger will be done by using S0 and S1 counters. No modification is needed in the double analyzer polarimeter which will be used with two CH_2 analyzers.

7.4 The DAQ for the Calorimeter

The DAQ of the calorimeter, constructed for experiment E04-108, will have almost all components required in the proposed experiment. The coincidence logic between proton and photon arms also will be assembled. In experiment E99-114 the DAQ and HV crates of the calorimeter were located in Hall A near the outer wall at angle of 60° and shielded by 10 inches of the concrete walls from the target and beam dump sides. The trip rate of the

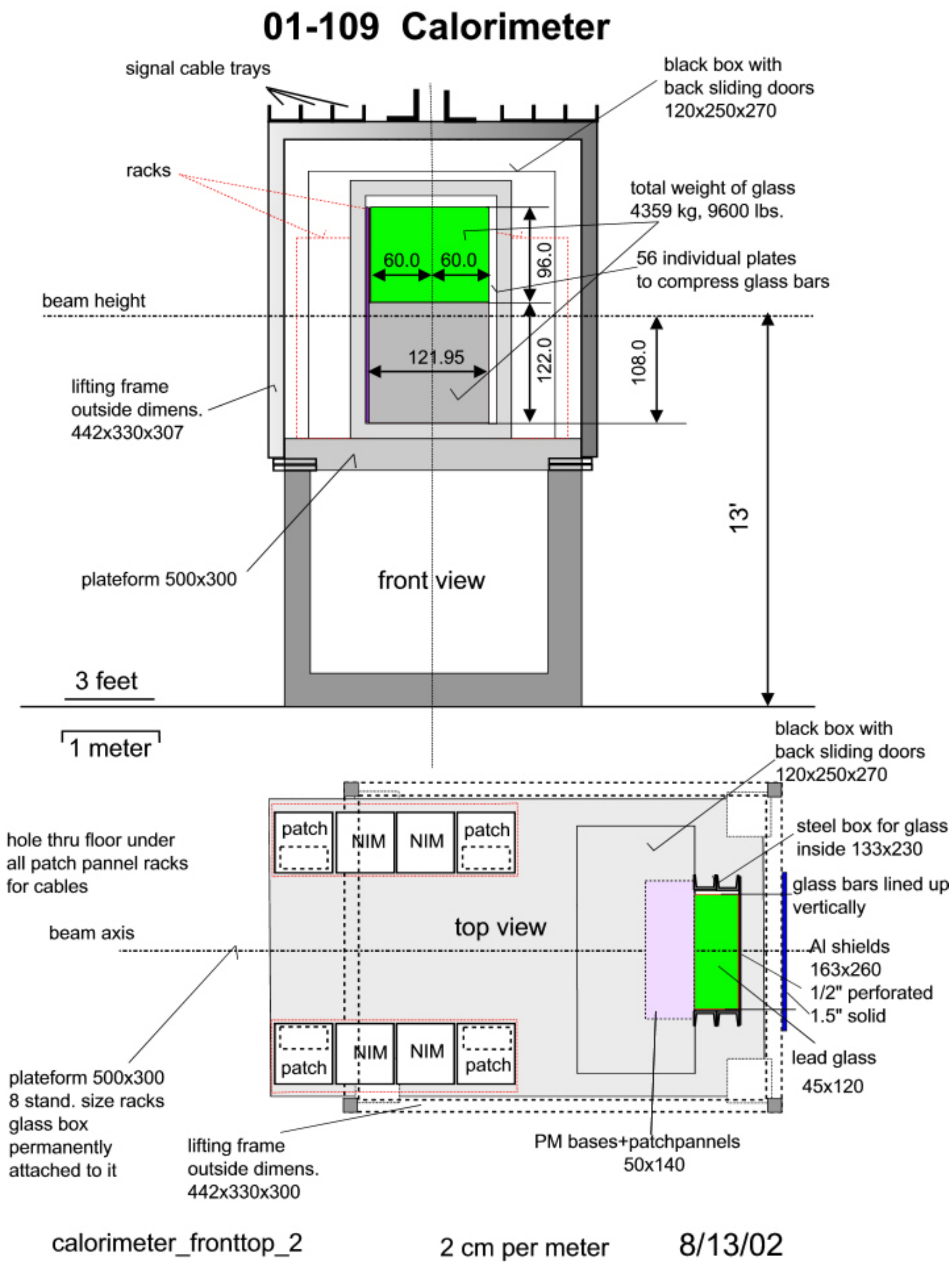

Figure 20: The structure of the BigCal calorimeter and layout of the support stand [35].

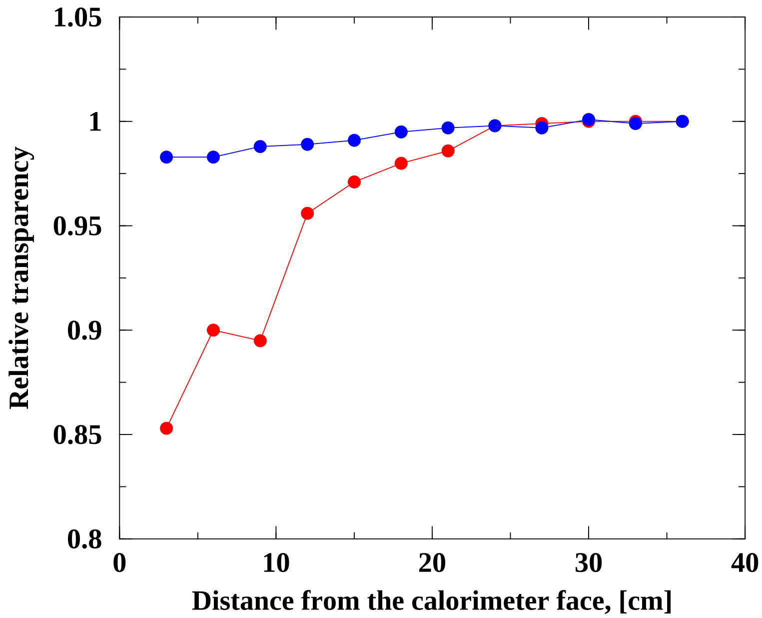

Figure 21: Transparency of lead glass blocks used in E99-114 before (red) and after UV annealing (blue).

CPU was about 1-2 per shift. To mitigate the trip problem we will increase thickness of shielding by an additional 8 inches of concrete or move the DAQ to the 105° position, where the radiation is about 15 times less, according to our calculation and measurements.

8 Conclusions

We request 508 hours of beamtime to measure the longitudinal and transverse components of the polarization transfer in RCS at $s= 9$ (GeV/c)^2 for $\theta_p^{cm} = 90$ and $110°$. This experiment will take place in Hall A for 508 hours, utilizing the polarized electron beam and HRS-left spectrometer with the focal plane polarimeter to detect protons, and BigCal calorimeter to detect scattered photons.

Knowledge of the polarization transfer in RCS at these kinematics will allow a rigirous test of the reaction mechanism for exclusive reactions at high t, which is crucial for the understanding of nucleon structure. We propose to measure polarization transfer K_{LL} in each kinematical point to a statistical accuracy of ± 0.06. Simultaneously the polarization observable P_N will be measured to a statistical accuracy of $\pm(0.10 - 0.15)$, and the polarization observable K_{LT} will be measured to a statistical accuracy of ± 0.05.

References

[1] A.V. Radyushkin, *Phys. Rev.* **D 58**, 114008 (1998).

[2] M. Diehl, T. Feldmann, R. Jakob, P. Kroll, *Eur. Phys. J.* **C 8**, 409 (1999).

[3] H. W. Huang, P. Kroll, T. Morii, *Eur. Phys. J.* **C 23**, 301 (2002).

[4] G. R. Farrar and H. Zhang, *Phys. Rev. Lett.* **41**, (1990) 1721, *Phys. Rev.* **D 65** (1990) 3348.

[5] A. S. Kronfeld and B. Nizic, *Phys. Rev.* **D 44**, 3445 (1991).

[6] M. Vanderhaeghen, P. A. M. Guichon and J. Van de Wiele, *Nucl. Phys.* **A 622**, 144c (1997).

[7] T. Brooks and L. Dixon, *Phys. Rev.* **D 62** 114021 (2000).

[8] R. Thomson, Alex Pang, and Cheng-Ryong Ji, *Phys. Rev.* **D 73** 054023 (2006).

[9] D.M. Scott, *Phys. Rev.* **D 10** 3117 (1974).

[10] P. Kroll *et al.*, *Phys. Lett* **B 316** 546 (1993).

[11] F. Cano and J. M. Laget, *Phys. Rev.* **D 65**, 074022 (2002)

[12] C. Hyde-Wright, A. Nathan, and B. Wojtsekhowski, spokespersons, JLab experiment E99-114.

[13] D. J. Hamilton, V. H. Mamyan *et al.*, *Phys. Rev. Lett.* **94**, 242001 (2005).

[14] R. Gilman, A. Nathan, and B. Wojtsekhowski, spokespersons, JLab experiment E07-002.

[15] D. Day and B. Wojtsekhowski, spokespersons, JLab experiment E05-101.

[16] M. Diehl *et al.*, *Phys. Rev.* **D 67**, 037502 (2003).

[17] G. A. Miller, *Phys. Rev.* **C 69**, 052201(R) (2004).

[18] F. Cano and J. M. Laget, *Phys. Lett.* **B 551**, 317 (2003).

[19] X. Ji, *Phys. Rev.* **D 55**, 7114 (1997), *Phys. Rev. Lett.* **78**, 610 (1997).

[20] A.V. Radyushkin, *Phys. Lett.* **B 380**, 417 (1996), *Phys. Rev.* **D 56**, 5524 (1997).

[21] M. Jones *et al.*, *Phys. Rev. Lett.* **84**, 1398 (2000).

[22] O. Gayou *et al.*, *Phys. Rev. Lett.* **88**, 092301 (2002).

[23] G. A. Miller and M. R. Frank, *Phys. Rev.* **C 65**, 065205 (2002)

[24] G. A. Miller, *Phys. Rev.* **C 66**, 032201 (2002)

[25] S. J. Brodsky and G. P. Lepage in *Perturbative Quantum Chromodynamics*, edited by A. Mueller (World Scientific, Singapore, 1989).

[26] S. J. Brodsky and G. Farrar, *Phys. Rev. Lett.* **31**, 1953 (1973).

[27] V. Matveev *et al.*, *Nuovo Cimento Lett.* **7**, 719 (1973).

[28] S. J. Brodsky and G. P. Lepage, *Phys. Rev.* **D 22**, 2157 (1980).

[29] K. Wijesooriya *et al.*, *Phys. Rev. C***66**, 034614 (2002).

[30] M. A. Shupe *et al.*, *Phys. Rev.* **D 19**, 1921 (1979).

[31] E. Lomon, *Phys. Rev.* **C 66**, 045501 (2002).

[32] R. L. Anderson *et al.*, *Phys. Rev.* **D 14**, 679 (1976).

[33] M. Battaglieri *et al.*, *Phys. Rev. Lett.* **87**, 172002 (2001).

[34] T. H. Bauer, *et al.*, *Rev. Mod. Phys.* **50**, 261 (1978).

[35] C. Perdrisat *et al.*, JLab experiment E01-109, 2001.

[36] B. Bonin *et al.*, *Nucl. Instr. Meth.* **A 288**, 379 (1991).

[37] I. M. Sitnik *et al.*, private communication, 2002.

[38] A. I. Akhiezer and M. P. Rekalo, *Sov. J. Nucl. Phys.* **3**, 277 (1974).

[39] R. Arnold, C. Carlson and F. Gross, *Phys. Rev.* **C 23**, 363 (1981).

[40] C. Perdrisat and L. Pentchev, private communtication, 2002.

[41] V. L. Chernyak and A. R. Zhitnitsky, *Phys. Rep.* **112**, 173 (1984).

[42] V. L. Chernyak, A. A. Oglobin, and A. R. Zhitnitsky, *Z. Phys.* **C 42**, 569 (1989).

[43] I. D. King and C. T. Sachrajda, *Nucl. Phys.* **A 598**, 785 (1987).